C. elegans CLASP/CLS-2 negatively regulates membrane ingression throughout the oocyte cortex and is required for polar body extrusion

Aleesa J. Schlientz[1] and Bruce Bowerman[1]

Institute of Molecular Biology, University of Oregon, Eugene, OR 97403

[1]Institute of Molecular Biology, 1229 University of Oregon, Eugene, Oregon 97403, USA

*Corresponding author (bowerman@uoregon.edu)

Short Title: Spindle structure and polar body extrusion

Abstract

The requirements for oocyte meiotic cytokinesis during polar body extrusion are not well understood. In particular, the relationship between the oocyte meiotic spindle and polar body contractile ring dynamics remains largely unknown. We have used live cell imaging and spindle assembly defective mutants lacking the function of CLASP/CLS-2, kinesin-12/KLP-18, or katanin/MEI-1 to investigate the relationship between meiotic spindle structure and polar body extrusion in *C. elegans* oocytes. We show that spindle bipolarity and chromosome segregation are not required for polar body contractile ring formation and chromosome extrusion in *klp-18* mutants, but oocytes with severe spindle assembly defects due to loss of CLS-2 or MEI-1 have penetrant and distinct polar body extrusion defects: CLS-2 is required early for contractile ring assembly or stability, while MEI-1 is required later for contractile ring constriction. We also show that CLS-2 negatively regulates membrane ingression throughout the oocyte cortex during meiosis I, and we explore the relationship between global cortical dynamics and oocyte meiotic cytokinesis.

Author Summary

The precursor cells that produce gametes—sperm and eggs in animals—have two copies of each chromosome, one from each parent. These precursors undergo specialized cell divisions that leave each gamete with only one copy of each chromosome; defects that produce incorrect chromosome number cause severe developmental abnormalities. In oocytes, these cell divisions are highly asymmetric, with extra chromosomes discarded into small membrane bound polar bodies, leaving one chromosome set within the much larger oocyte. How oocytes assemble the contractile apparatus that pinches off polar bodies remains poorly understood. To better understand this process, we have used the nematode *Caenorhabditis elegans* to investigate the relationship between the bipolar structure that separates oocyte chromosomes, called the spindle, and assembly of the contractile apparatus that pinches off polar bodies. We used a comparative approach, examining this relationship in three spindle assembly defective mutants. Bipolar spindle assembly and chromosome separation were not required for polar body extrusion, as it occurred normally in mutants lacking a protein called KLP-18. However, mutants lacking the protein CLS-2 failed to assemble the contractile apparatus, while mutants lacking the protein MEI-1 assembled a contractile apparatus that failed to fully constrict. We also found that CLS-2 down-regulates membrane ingression throughout the oocyte surface, and we explored the relationship between oocyte membrane dynamics and polar body extrusion.

Introduction

Oocyte meiosis comprises a single round of genome replication followed by two highly asymmetric cell divisions that produce a single haploid gamete and two small polar bodies that contain discarded chromosomes (1-4). An acentrosomal spindle segregates homologous chromosomes during the first reductional division, called meiosis I, and half of the recombined homologs are extruded into the first polar body. The equational meiosis II division then segregates sister chromatids, with half extruded into a second polar body and half remaining in the oocyte cytoplasm. Despite being essential for reducing oocyte ploidy, little is known about the cues that organize and influence the actomyosin contractile ring that mediates polar body extrusion.

The oocyte contractile ring initially forms distal to the membrane-proximal meiotic spindle pole, with the spindle axis oriented orthogonally to the overlying cell cortex (5). During anaphase the contractile ring ingresses past both the membrane-proximal pole and one set of the segregating chromosomes to then constrict and ultimately separate the nascent polar body from the oocyte. These dynamics contrast substantially with mitotic cytokinesis (Fig 1A), during which signals from astral microtubules and the central spindle position the contractile ring midway between the two spindle poles (6-8). While the signals required for contractile ring assembly and constriction during mitotic cytokinesis are relatively well understood, how oocyte meiotic spindles influence contractile ring dynamics during polar body extrusion is not known.

In *Caenorhabditis elegans*, several genes are required for polar body extrusion, but how their functions are coordinated remains poorly understood. Similar to mitotic cytokinesis, polar body cytokinesis requires filamentous actin and the non-muscle

myosin II heavy-chain NMY-2 and light-chains MLC-4 and MLC-5 (9-11). The cytoskeletal scaffolding protein anillin/ANI-1 facilitates transformation of the initial actomyosin contractile ring into a midbody tube, with anillin depletion resulting in large and unstable polar bodies that often fuse with the oocyte (12). Consistent with its role as a key activator of cortical actomyosin, the small GTPase RhoA (RHO-1) and its RhoGEF ECT-2 also are required for oocyte polar body extrusion (10, 13). Knockdown of the centralspindlin complex, comprised of MgcRacGAP/CYK-4 and kinesin-6/ZEN-4, results in the assembly of abnormally large contractile rings and a subsequent failure in extrusion (10). Finally, the chromosomal passenger complex (CPC) member Aurora B/AIR-2 also is required (14).

Formation of the contractile ring distal to both meiotic spindle poles raises the question of how the ring moves relative to the spindle such that it constricts midway between segregating chromosomes. One mechanism proposed for *C. elegans* is that global contraction of actomyosin throughout the oocyte cortex produces a hydrostatic cytoplasmic force that, combined with depletion of cortical actomyosin overlying the membrane-proximal pole, leads to an out-pocketing of the membrane within the contractile ring and pushes the spindle into the protruding pocket (10, 15). In support of this hypothesis, increased global cortical contractility due to depletion of casein kinase 1 gamma (CSNK-1), a negative regulator of RhoA activity, often results in extrusion of the entire meiotic spindle (15). However, assessing whether global cortical contractility is required for polar body extrusion has been challenging due to the overlap in requirements for global cortical contractility and polar body contractile ring assembly and constriction.

Despite a stereotyped spatial relationship between the oocyte meiotic spindle and contractile ring assembly and ingression, little is known about how the spindle might influence ring assembly and dynamics. Nevertheless, four observations suggest that the meiotic spindle provides important cues. First, meiotic spindles that fail to translocate to the oocyte cortex induce the formation of membrane furrows that ingress deeply towards the displaced spindle (10). Second, loss of the centralspindlin complex, which localizes to the central spindle during anaphase, results in the formation of rings with an abnormally large diameter (10). Third katanin/*mei-1* mutants, which assemble apolar spindles, produce very large polar bodies (16, 17) . Finally, while work in mice suggests that chromosomes themselves may provide cues for ring assembly and polar body extrusion via the small GTPase Ran (18, 19), knock down of *C. elegans* RAN-1 does not prevent polar body extrusion (20, 21). These findings suggest that in *C. elegans* the oocyte meiotic spindle provides cues that influence contractile ring assembly and ingression.

To explore the relationship between meiotic spindle assembly and polar body extrusion, we have examined oocyte cortical actomyosin dynamics in three spindle assembly defective mutants that each lack the function of a conserved protein: CLASP/CLS-2, kinesin-12/KLP-18, or katanin/MEI-1 (Fig 1B). CLASP family proteins promote microtubule stability through their association with microtubules and their tubulin heterodimer-binding TOG (Tumor Over-expressed Gene) domains, decreasing the frequency of microtubule catastrophe and promoting rescue of de-polymerizing microtubules (22-25). Moreover, human CLASPs have been shown to influence not only microtubule stability and dynamics, but also to interact with actin filaments and

potentially crosslink filamentous actin and microtubules (26). CLS-2 is one of three *C. elegans* CLASPs and is required for mitotic central spindle stability as well as oocyte meiotic spindle assembly and chromosome segregation (27-30). Vertebrate kinesin-12/KLP-18 family members promote mitotic spindle bipolarity by contributing to forces that push apart anti-parallel microtubules (31-33). Consistent with such a function, *C. elegans* oocytes lacking the kinesin-12 family member KLP-18 form monopolar meiotic spindles that draw chromosomes towards a single spindle pole and thus fail in chromosome segregation (34-36). The widely conserved microtubule severing complex katanin is encoded by two *C. elegans* genes, *mei-1* and *mei-2* (37, 38). Loss of either subunit results in the formation of apolar meiotic spindles that fail to congress or segregate chromosomes (34, 39, 40).

Here we report our use of fluorescent protein fusions and live cell imaging to characterize polar body extrusion during meiosis I in mutants lacking the function of CLS-2, KLP-18 or MEI-1. Previous studies indicate that both CLS-2 and MEI-1 are involved in polar body extrusion, with oocytes lacking CLS-2 frequently failing to extrude polar bodies (27, 30, 41), and oocytes lacking MEI-1 forming very large polar bodies (16, 17, 42, 43). Furthermore, *klp-18* mutants sometimes lack an oocyte pronucleus, suggesting that all oocyte chromosomes can be extruded (34). However, the process of polar body extrusion has not been directly examined in any of these mutants. Our live imaging of contractile ring assembly and ingression in these mutant backgrounds shows that bipolar spindle assembly and chromosome segregation are not required for oocyte contractile ring assembly and polar body extrusion. However, CLS-2 is required for proper contractile ring assembly or stability and also acts as a negative regulator of

145 global cortical membrane ingressions, while MEI-1 may be required late in polar body
146 extrusion for contractile ring constriction.
147
148 **Results**
149 **CLS-2 is required for oocyte meiotic spindle assembly and polar body extrusion**
150 To investigate the role of CLS-2, we first examined the localization of a CLS-
151 2::GFP fusion in live oocytes (Fig 2A, S1 Fig, S1 and S2 Movies). Consistent with
152 previous reports, CLS-2::GFP initially localized to meiosis I spindle microtubules and
153 kinetochore cups, and to small patches dispersed throughout the oocyte cortex (27, 30,
154 41). Around the time of anaphase onset, the cortical CLS-2::GFP patches disappeared
155 and CLS-2::GFP localized to the central spindle between the segregating chromosomes
156 (27, 30, 41). These results suggest that CLS-2 might have roles not only at the oocyte
157 meiotic spindle but also throughout the oocyte cortex.
158 Previous studies of CLS-2 requirements have used RNA interference (RNAi) or
159 auxin-induced degradation of degron-tagged CLS-2 to reduce its function and have
160 emphasized its central spindle function. To more definitively assess its roles during
161 oocyte meiosis, we used CRISPR/Cas9 to generate putative null alleles. Each of the
162 four alleles we isolated contains small insertions or deletions that result in frame shifts
163 and premature stop codons before the first TOG domain, likely making them null (Fig
164 2B, S1 Fig). All are recessive, and homozygous mutant hermaphrodites exhibit fully
165 penetrant embryonic lethality (Fig 2C). To investigate CLS-2 requirements, we have
166 used the *cls-2(or1948)* allele, and hereafter we refer to oocytes from homozygous *cls-*
167 *2(or1948)* hermaphrodites as *cls-2* mutants.

We first used *ex utero* live cell imaging with transgenic strains that express GFP fused to a β-tubulin (GFP::TBB-2) and mCherry fused to a histone H2B (mCherry::H2B) to examine microtubule and chromosome dynamics during meiosis I in control and *cls-2* mutant oocytes (Fig 2D; see Materials and methods). Control oocytes formed barrel shaped bipolar spindles that shortened and rotated to become perpendicular to the oocyte cortex prior to anaphase and polar body extrusion (n=19). Consistent with previous reports (27, 30, 41), the meiosis I spindles in *cls-2* mutants were disorganized and lacked any obvious bipolarity, with chromosomes moving into a small cluster before failing to segregate (n=13). Furthermore, microtubule levels appeared to be reduced, and quantification of the integrated spindle microtubule intensity over time showed a substantial reduction in microtubule levels throughout meiosis I compared to control oocytes (Fig 2E), consistent with the established roles of CLASP family members in promoting microtubule stability (see Introduction). To assess when defects in meiosis I spindle assembly first appear in *cls-2* oocytes, we used *in utero* live cell imaging and observed the early assembly of a normal cage-like microtubule structure that surrounded the oocyte chromosomes, followed by a rapid collapse of this microtubule structure to form an abnormally small cluster associated with the oocyte chromosomes (S1 Fig) (n=5). To further examine spindle assembly in *cls-2* mutants, we also imaged meiosis I in oocytes from transgenic strains expressing an endogenous fusion of GFP to the pole marker ASPM-1 and mCherry::H2B (Fig 2F). As described previously (44), multiple small GFP::ASPM-1 foci coalesced to form a bipolar spindle in control oocytes (n=14). In *cls-2* mutants, the GFP::ASPM-1 foci failed to coalesce to form two spindle poles but rather moved over time to form a single tight cluster of multiple small foci, and

chromosomes again moved into a small cluster and failed to segregate (n=11). We conclude that CLS-2 plays an important role in promoting microtubule stability throughout meiosis I and is required early in bipolar spindle assembly and for chromosome segregation.

In addition to the extensive meiotic spindle defects, we also observed that *cls-2* mutants frequently failed to extrude a polar body at the end of meiosis I, consistent with previous reports (27, 30). Control oocytes regularly extruded a polar body at the end of meiosis I, as scored using transgenic strains expressing either GFP::H2B or mCherry::H2B and observing whether oocyte chromosomes remained extruded for the duration of live imaging (93 of 94 oocytes; Fig 2G). In contrast, polar body extrusion failed in about 84% of the *cls-2* mutant oocytes (80 of 95, Fig 2G). This finding suggests that CLS-2 might play a direct role in polar body extrusion, or that the spindle defects observed in *cls-2* mutants might indirectly disrupt extrusion.

Polar body extrusion defects in *cls-2* mutants are not due to absence of the central spindle-associated proteins AuroraB/AIR-2 or MgcRacGAP/CYK-4

Because *cls-2* mutant oocytes fail to assemble a central spindle or segregate chromosomes and CLS-2::GFP localizes to the central spindle, and because the central spindle-associated protein AuroraB/AIR-2 and the centralspindlin component MgcRacGAP/CYK-4 are required for polar body extrusion (10, 14, 27, 45), we first considered whether the polar body extrusion defects might be due to a failure to localize central spindle proteins to the disorganized spindle microtubules in *cls-2* oocytes. To address this possibility, we used transgenic strains expressing GFP fusions to either

AIR-2 or CYK-4 and examined their localization in control and *cls-2* mutant oocytes. As reported previously, both proteins localized to the central spindle during anaphase in control oocytes (Figs 3A and 3B) (n=12 GFP::AIR-2 and n=12 CYK-4::GFP). In *cls-2* mutants, despite the lack of spindle organization, both AIR-2 and CYK-4 localized to the spindle region (Figs 3A and 3B) (n=15 GFP::AIR-2 and n=11 CYK-4::GFP). While we cannot rule out the possibility that improper localization of AIR-2 and CYK-4 to the defective spindle might be responsible for the failure to extrude polar bodies in *cls-2* mutants, this failure cannot be explained by a simple loss of these central spindle-associated proteins from the mutant spindle microtubules.

CLS-2 and MEI-1, but not spindle bipolarity, are required for polar body extrusion

Because the relationship between spindle structure and polar body extrusion is unclear, we next took a comparative approach and also examined meiosis I polar body extrusion after using RNAi to knock down either kinesin-12/KLP-18 or katanin/MEI-1. As illustrated schematically in Fig 1B, *klp-18* mutants assemble monopolar spindles while *mei-1* spindles are apolar, and both fail to segregate chromosomes (see Introduction). We first simply assessed whether polar body extrusion was successful, again using live imaging with transgenic strains expressing either GFP::H2B or mCherry::H2B fusions and scoring whether chromosomes were retained in polar bodies for the duration of imaging (Fig 2G). In *klp-18* mutants, chromosomes were successfully retained in a polar body in 15 of 20 oocytes. In contrast, after MEI-1 knockdown, chromosomes were extruded and retained in a polar body in only 5 of 27 oocytes. The absence of meiosis I polar body extrusion in *mei-1* mutant oocytes was surprising because *mei-1* mutants

were originally described as typically having abnormally large polar bodies (16, 17), but how often polar body extrusion succeeds or fails has not been reported. Our data indicate that meiosis I polar body extrusion usually fails and suggest that the abnormally large polar bodies observed in *mei-1* mutants result from defects in meiosis II (see Discussion).

Based on the frequent success of polar body extrusion in *klp-18* mutants, we conclude that spindle bipolarity and chromosome segregation are not required for polar body extrusion. Thus, the failed extrusions in *cls-2* and *mei-1* mutants are not simply due to an absence of spindle bipolarity or a failure to segregate chromosomes.

Meiotic spindle-associated furrows are abnormal in *cls-2 and mei-1* mutant oocytes

To better understand the polar body extrusion defects in oocytes lacking CLS-2 or MEI-1, we next examined the spindle-associated membrane furrows that mediate polar body extrusion in transgenic strains expressing mCherry fused to a plasma membrane marker (mCherry::PH) and GFP::H2B (Figs 4A and 4B, S2 Fig, S3 and S4 Movies). In 9 of 16 control oocytes, we observed early membrane furrows that ingressed until they pinched together to encapsulate and extrude chromosomes into the first polar body. In 6 of 16 control oocytes we observed early membrane furrows that were not as clearly resolved in our imaging data but eventually led to polar body extrusion, and in one oocyte furrows were not obvious but a polar body was nevertheless extruded.

In contrast, we observed extensive spindle-associated membrane furrowing defects in *cls-2* mutants (Figs 4C-E, S3 and S4 Figs, S5 and S6 Movies). In 7 of 19 oocytes we observed two furrows in cross-section that retracted before pinching together, one oocyte that formed two furrows that pinched together but failed late in polar body extrusion, and one oocyte that formed two furrows and successfully extruded a polar body (S3 Fig). One of 19 oocytes appeared to form three spindle-associated furrows in cross-section and extruded a polar body (S3 Fig). In 7 of 19 oocytes we observed only a single visible spindle-associated furrow in cross-section that ingressed either to one side of, or directly toward the oocyte chromosomes (Fig 4D, S4 Fig), suggesting that the contractile ring collapsed into a more linear ingressing structure rather than maintaining a ring-like shape. Finally, in one oocyte the membrane dynamics were indistinct, but chromosomes were extruded into a polar body (Fig 4E), and in one oocyte there was no obvious spindle-associated furrowing and polar body extrusion failed (S4 Fig).

In oocytes depleted of *klp-18*, we observed furrows that more nearly resembled those in control oocytes (Figs 4F and G, S5 Fig, S7 and S8 Movies). In 4 of 10 oocytes, we observed two furrows in cross-section that ingressed more deeply and then pinched together (Fig 4F), and only 1 of these 4 failed in polar body extrusion. In 6 of 10 oocytes, we observed shallow furrows adjacent to the oocyte chromosomes (Fig 4G), and only 1 of these 6 failed to extrude a polar body.

After MEI-1 knockdown, we observed furrows that initially resembled those in control oocytes but were more widely spaced and often failed late during constriction (Figs 4H-J, S6 Fig, S9 and S10 Movies). In 2 of 11 oocytes, we observed two furrows in

cross-section that ingressed and pinched together to extrude a polar body (Fig 4H). In 3 of 11 oocytes two furrows ingressed and pinched together but then regressed and released chromosomes back into the oocyte cytoplasm (Fig 4I). In 5 of 11 oocytes two furrows ingressed but retracted before pinching together and failed in polar body extrusion (Fig 4J), and finally in 1 of 11 oocytes we observed only a single spindle-associated furrow in cross-section that failed to extrude a polar body.

To summarize, in *klp-18* mutant oocytes we observed spindle-associated furrows that usually encapsulated chromosomes and extruded polar bodies, although the oocyte chromosomes were often in close proximity to the membrane with furrows that were shallow and difficult to detect. In *cls-2* and *mei-1* mutants, meiosis 1 polar body extrusion frequently failed but we observed distinct defects. While membrane furrowing initially appeared normal but eventually failed in most *mei-1* mutant oocytes, *cls-2* oocytes often appeared abnormal early in furrow ingression and exhibited more severe defects as extrusion attempts progressed.

Polar body contractile ring dynamics are more severely defective in the absence of CLS-2 than in *klp-18* or *mei-1* mutant oocytes.

We next examined assembly and ingression of the contractile ring during oocyte meiosis I, using live cell imaging with transgenic strains expressing both a GFP fusion to the non-muscle myosin II NMY-2 and mCherry::H2B. In 11 of 11 control oocytes, NMY-2::GFP foci initially assembled into discontinuous but discernible rings over the membrane proximal pole, after spindle rotation and before extensive chromosome segregation, and then became more continuous and prominent as they ingressed and

305 constricted between the segregating chromosomes to extrude polar bodies (Fig 5A, S7
306 Fig, S11 and S12 Movies).

307 In *cls-2* mutant oocytes, the assembly and stability of NYM-2::GFP contractile
308 ring structures were severely defective (Fig 5B, S8 Fig, S13 and S14 Movies). In 7 of 11
309 oocytes, fragmented or partial contractile rings assembled and 6 of these oocytes failed
310 to extrude a polar body, while 3 of 11 oocytes formed abnormal assemblies of
311 NMY2::GFP that were more linear and not ring-like, although 2 of these extruded a
312 polar body. Finally, 1 of 11 oocytes formed a relatively normal looking contractile ring
313 that extruded a polar body. The fragmented or partial contractile rings observed in *cls-2*
314 mutants often collapsed into single bright foci or bands during constriction.

315 Contractile ring assembly and dynamics appeared much more normal in *klp-18*
316 mutant oocytes (Fig 5C, S9 Fig, S15 and S16 Movies). In 10 of 10 oocytes after KLP-18
317 knockdown, NMY-2::GFP foci assembled into rings that ingressed and constricted with
318 dynamics similar to those observed in control oocytes, and in 9 of the 10 oocytes
319 chromosomes were stably extruded into polar bodies.

320 In MEI-1 knockdown oocytes, ring assembly and ingression were much more
321 normal compared *to cls-2* mutants, but we nevertheless observed a range of later
322 defects and eventual failures to extrude polar bodies (Fig 5D, S10 Fig, S17 and S18
323 Movies). In 11 of 13 oocytes, the NMY-2::GFP rings that initially formed were larger in
324 diameter compared to control oocytes, and in 3 of these 11 oocytes the rings
325 constricted and successfully extruded a polar body. In another 5 of these 11 oocytes,
326 the rings constricted extensively but ultimately regressed and failed at polar body
327 extrusion, while in 3 the rings ingressed and only constricted partially before regressing

328 and failing to extrude polar bodies. Finally, in 2 of 13 oocytes, ring assembly and
329 ingression were more defective and polar body extrusion failed.
330 To further characterize the polar body extrusion defects in *cls-2* mutants, we also
331 examined ring assembly and dynamics in transgenic strains expressing mNeonGreen
332 fused to the anillin ANI-1 (mNG::ANI-1), which is dispensable for assembly of the
333 actomyosin contractile ring but required for its conversion from a ring to a tube during
334 constriction (46), and mCherry::H2B (Fig 6A, S19 and S20 Movies). In 10 of 10 control
335 oocytes, mNG::ANI-1 assembled into contractile rings that ingressed and constricted
336 between segregating chromosomes to extrude a polar body, while in 10 of 10 *cls-2*
337 oocytes a fragmented contractile ring structure formed and failed to extrude a polar
338 body. We also used two-color live imaging to examine NMY-2::mKate2 and mNG::ANI-1
339 simultaneously, and observed that these two contractile ring components were co-
340 localized in both control and *cls*-2 mutant oocytes (Fig 6B, S21 and S22 Movies) (n=11
341 control, n=13 *cls-2(or1948)*). We conclude that CLS-2 is required for proper ring
342 assembly and ingression dynamics of not only NMY-2 but also ANI-1.
343
344 **CLS-2 negatively regulates membrane ingression throughout the oocyte cortex**
345 **during meiosis I**
346 Global contraction of the oocyte actomyosin cortex has been proposed to
347 promote polar body extrusion by generating a hydrostatic cytoplasmic force that (i)
348 produces an out-pocketing of the actomyosin depleted membrane inside the meiotic
349 contractile ring, and (ii) pushes the spindle partially into the extruded membrane pocket
350 (see Introduction). To explore the relationship between spindle structure, global cortical

351 contractility and polar body extrusion, we next examined membrane ingressions
352 throughout the oocyte cortex during meiosis I in control and mutant oocytes, using
353 transgenic strains expressing mCherry::PH and GFP::H2B fusions. To document these
354 membrane ingressions, we used temporal overlays of a single central z-plane to portray
355 simultaneously the membrane position at all time points throughout the period of global
356 cortical furrowing. In control oocytes, we observed the spindle-associated furrows and a
357 small number of additional furrows along the oocyte cortex (Fig 7A, S11 Fig) (n=16).
358 In contrast, *cls-2* mutant oocytes exhibited more extensive cortical furrowing
359 compared to control oocytes (n=24), while oocytes depleted of either KLP-18 or MEI-1
360 more nearly resembled control oocytes (Fig 7A, S12 and S13 Figs, S3-10 Movies)
361 (n=10 *klp-18(RNAi)* and n=14 *mei-1(RNAi)*). Quantification of global cortical furrowing
362 showed that *cls-2* oocytes had significantly more furrows compared to control and *klp-*
363 *18* oocytes (Fig 7B). We conclude that CLS-2 negatively regulates global cortical
364 furrowing, and we suspect that the CLS-2::GFP patches detected throughout the oocyte
365 cortex are responsible for this regulation (Fig 2A, S1 Fig, S1 and S2 Movies; see
366 Discussion).
367 We next examined the dynamics of the cortical actomyosin cytoskeleton, which
368 mediates the furrowing that occurs throughout the oocyte cortex during polar body
369 extrusion. In control oocytes, NMY-2 and ANI-1 localized to dynamic patches
370 throughout the oocyte cortex during meiosis I contractile ring assembly and ingression,
371 and then dissipated late in anaphase when global cortical furrowing ends (Figs 7C and
372 7D, S14 and S15 Figs, S23 and S24 Movies) (n=11 NMY-2::GFP, n=10 mNG::ANI-1).
373 To determine if the increased global cortical furrowing in *cls-2* oocytes is caused by an

increase in NMY-2 or ANI-1 patch size or duration, we examined the dynamics of NMY-2::GFP and mNG::ANI-1 and observed dynamics similar to those in control oocytes (Figs 7C and 7D, S16-18 Figs, S25 and S26 Movies) (n=11 NMY-2::GFP, n=10 mNG::ANI-1), and we did not detect any statistically significant difference in the area occupied by the cortical NMY-2::GFP patches throughout the period of global cortical furrowing and polar body extrusion. These data suggest that the excess global cortical furrowing observed in *cls-2* oocytes is not due to altered NMY-2 or ANI-1 patch dynamics. While the increased global cortical furrowing in CSNK-1 knockdown oocytes is associated with altered NMY-2 and ANI-1 cortical patch dynamics and with extrusion of the entire meiosis I spindle into polar bodies (15), the increased global cortical furrowing in *cls-2* mutants does not correlate with altered cortical patch dynamics and is instead associated with polar body extrusion failure. Thus, the relationship between global cortical furrowing and polar body extrusion is complex and requires further investigation (see Discussion).

Discussion

Remarkably little is known about the relationship between spindle structure and contractile ring assembly and constriction during oocyte meiotic cell division. To gain insight into the cues that influence contractile ring dynamics during polar body extrusion, we have examined contractile ring assembly and constriction in three different *C. elegans* spindle assembly-defective mutants. Our results indicate that the *C. elegans* CLASP family member CLS-2 is required not only for assembly of a bipolar meiosis I spindle and for chromosome segregation, but also for an early stage in oocyte meiosis I

contractile ring assembly or stability. This requirement for CLS-2 is not due simply to a failure in assembling bipolar spindles or to a lack of chromosome segregation, because *klp-18/kinesin-12* mutant oocytes formed monopolar spindles and failed to segregate chromosomes but did assemble stable contractile rings that usually extruded chromosomes into a polar body. We have further shown that *mei-1/katanin* mutant oocytes, which assemble apolar and disorganized oocyte meiosis I spindles, also usually failed to extrude polar bodies. However, while CLS-2 was required early for contractile ring assembly or stability, MEI-1 appears to be required to limit the initial diameter of the contractile ring and for later steps in ring constriction. Finally, we also observed increased global cortical furrowing during meiosis I in *cls-2* mutant oocytes but not in *klp-18* or *mei-1* mutants, raising the possibility that proper regulation of cortical membrane ingressions throughout the oocyte may be required for contractile ring assembly or stability during polar body cytokinesis. Our results highlight the value of exploring the relationship between mutant oocyte meiotic spindle structures and polar body contractile ring dynamics.

Using spindle assembly defective mutants to explore contractile ring dynamics during oocyte polar body extrusion

While the requirements for several factors that control oocyte meiotic spindle assembly in *C. elegans* have been described (1-3), the impact of the resulting spindle assembly defects on polar body extrusion has remained largely unexplored. Indeed, anecdotal observations have suggested that polar body extrusion can occur even in mutants with severe oocyte spindle assembly defects. For example, reducing the

function of the microtubule severing complex katanin, comprised of MEI-1 and -2 in *C. elegans*, results in severely defective apolar spindles that have greatly reduced levels of microtubules and fail to organize or segregate chromosomes and yet often produce abnormally large polar bodies. However, the dynamics of contractile ring assembly, ingression and constriction in *mei-1/katanin* mutants has not been directly examined. Similarly, mutant oocytes lacking the kinesin-12 family member KLP-18 assemble monopolar spindles that fail to segregate chromosomes but often produce zygotes that completely lack an egg pronucleus, indicating that all of the oocyte chromosomes are sometimes extruded into polar bodies, but again the process of polar body extrusion in *klp-18* mutants has not been directly examined. In mouse oocytes, DNA-coated beads have been shown to promote the assembly of a polar body-like cortical protrusion, which requires the small GTPase Ran that mediates chromatin signaling and, if allowed to assemble a bead-associated spindle structure, can lead to successful extrusion (18, 19). However, knockdown of the *C. elegans* Ran family member RAN-1 does not prevent chromosome segregation or polar body extrusion (20, 21), suggesting that chromatin cues do not mediate contractile ring assembly. Moreover, meiotic spindles that fail to translocate to the oocyte cortex induce the formation of membrane furrows that ingress deeply toward the spindle (10), and *C. elegans* mutant oocytes lacking central spindle proteins have been shown to produce abnormally large contractile rings that often fail to extrude chromosomes into a polar body (10), suggesting that the oocyte meiotic spindle does influence ring assembly and function.

Given the critical roles of astral and central spindle microtubules in promoting the assembly of a contractile ring during mitosis (6-8), the distinct dynamics and geometry

of oocyte meiotic contractile rings compared to mitotic contractile rings (Fig 1A), and the indications that oocyte meiotic spindles influence contractile ring dynamics in *C. elegans,* we have characterized polar body extrusion in *C. elegans* mutants that are severely defective in oocyte spindle assembly. We were first motivated to do so based on our observation that *cls-2* oocytes frequently failed to extrude chromosomes, in contrast to anecdotal and indirect observations that other *C. elegans* mutants with severe oocyte meiotic spindle assembly defects can extrude chromosomes into polar bodies.

Because *cls-2* mutant oocytes failed to assemble bipolar spindles or segregate chromosomes, we also examined polar body extrusion in *klp-18/kinesin-12* mutant oocytes that assemble monopolar spindles and also fail to segregate chromosomes (34-36). In contrast to *cls-2* mutants, in which contractile ring assembly or stability and membrane ingression were severely defective, contractile ring assembly and ingression appeared much more normal in *klp-18* mutant oocytes and chromosomes were usually extruded into a polar body. We conclude that the defects in *cls-2* mutant oocytes are not due a failure to assemble a bipolar spindle or to segregate chromosomes, but rather reflect a more specific requirement for CLASP/CLS-2.

A specific requirement for CLS-2 is further supported by our analysis of oocyte meiotic contractile ring assembly and dynamics in *katanin/mei-1* oocytes, which assemble spindles that lack any polarity and completely fail to organize the dispersed oocyte chromosomes throughout meiosis I (34, 39, 40). Furthermore, similar to *cls-2* oocytes, microtubule levels are substantially reduced in *mei-1* mutant oocytes (47). Nevertheless, stable contractile rings usually formed in *mei-1* mutant oocytes, although

the rings appeared somewhat larger in diameter than in control oocytes, and we frequently observed extensive furrow ingressions that often enclosed the oocyte chromosomes but usually failed to complete constriction and regressed late in cytokinesis. We conclude that contractile rings can assemble and remain stable until late in polar body extrusion, even when oocyte meiotic spindle assembly is at least as severely defective as in *cls-2* mutant oocytes.

Roles for CLS-2 and MEI-1 in contractile ring assembly and constriction.

While our analysis indicates that CLS-2 is required early for the assembly or stability of the oocyte meiosis I contractile ring, we do not know if the defects reflect a direct or indirect requirement, or how CLS-2 functions at a molecular level to promote polar body extrusion. Consistent with studies showing that CLASP family members associate with microtubules and promote microtubule stability (22-25), *cls-2* mutant oocytes have reduced levels of spindle microtubules throughout meiosis I. Moreover, *cls-2* mutant oocytes fail to assemble bipolar spindles or segregate chromosomes, with ASPM-1 pole foci and chromosomes instead converging into a small amorphous cluster. While the contractile ring assembly defects we observed could be an indirect consequence of aberrant spindle assembly and structure, the more normal contractile ring dynamics observed in both *klp-18* and *mei-1* mutant oocytes suggest that CLS-2 has a more specific role in mediating ring assembly or stability. Notably, human CLASP proteins have been shown to associate with actin filaments and may cross-link microtubules and filamentous actin (26). Furthermore, mutations in the *Drosophila* CLS-2 ortholog Orbit/Mast cause spermatocyte cytokinesis defects that appear to result from

a loss of central spindle microtubules that normally promote assembly of the contractile ring (48). Thus, it is possible that the contractile ring assembly or stability defects in *cls-2* mutants are due to a loss of microtubule and microfilament interactions that require CLS-2.

Consistent with a role for CLS-2 in bridging spindle microtubules and cortical actin filaments, we observed CLS-2::GFP throughout the oocyte spindles at the time when contractile ring assembly begins. However, at the time that ring assembly begins, very few spindle microtubules have been observed in close proximity to the cell cortex (49). Biochemical studies of CLS-2 and its potential interactions with microtubules and actin filaments, along with higher resolution imaging of CLS-2, spindle microtubules and cortical microfilaments in oocytes may improve our understanding of how CLS-2 promotes the proper assembly and stability of the contractile ring during polar body extrusion.

Contractile ring dynamics during meiosis I were more normal after *mei-1* RNAi knockdown, but the furrows nevertheless often regressed and polar body extrusion usually failed. Previous studies have shown that partial loss of function mutations in *mei-1* result in abnormally large second polar bodies that are produced after meiosis II, as a result of decreased microtubule severing that is required for complete disassembly of the oocyte meiosis II spindle (42, 43). Our results provide the first systematic examination of polar body extrusion during meiosis I after depletion of katanin/MEI-1, and it is possible that the late failures in polar body cytokinesis that we observed also reflect a requirement for microtubule severing. Alternatively, similar defects are observed in oocytes lacking the centralspindlin components CYK-4 and ZEN-4 (10, 14,

27, 45), and it is possible that central spindle proteins are mis-regulated after MEI-1 knockdown. Further investigation of MEI-1 and its interactions with central spindle proteins may improve our understanding of this late requirement for MEI-1 during polar body extrusion.

Negative regulation of oocyte global cortical dynamics and its relationship to polar body extrusion

In addition to the defects in contractile ring dynamics during polar body extrusion in *cls-2* mutant oocytes, we also observed increased membrane ingressions throughout the oocyte cortex. Furthermore, we detected CLS-2::GFP in small patches throughout the cortex in control oocytes. These patches were present early in meiosis I but dissipated before anaphase chromosome segregation, prior to initiation of the membrane ingressions that occur during anaphase in wild-type oocytes. While the excessive global furrowing in *cls-2* mutants may result from loss of the cortical CLS-2 patches, if so then CLS-2 may act prior to the initiation of global cortical furrowing to down-regulate the ingressions. Alternatively, low levels of cortical CLS-2 that were not detected with our imaging methods might contribute to this negative regulation of membrane furrowing throughout the oocyte cortex.

The molecular mechanism by which cortical CLS-2 patches might down-regulate global membrane ingression during oocyte meiosis I is not clear. Our observations that NMY-2 and ANI-1 dynamics were not altered in *cls-2* oocytes suggests that the increased membrane ingression is not be due to an increase in cortical actomyosin contractility but perhaps is an indirect consequence of defects in the stiffness of the

oocyte cortex. The observations that CLASP orthologs can interact with both cortical microtubules and actin filaments may be consistent with such a role for CLS-2 (26). Moreover, oocyte polar body extrusion has been described as a bleb-like process, with local weakening of the actomyosin cytoskeleton inside the contractile ring promoting an out-pocketing of the membrane to form a polar body (5, 10). Studies of bleb formation in other cellular contexts have shown that microtubule destabilization can result in bleb formation (50-52). Thus, it is possible that loss of CLS-2 promotes membrane ingressions throughout the cortex due to destabilization of cortical microtubules and a corresponding decrease in cortical stiffness, although we have not yet detected statistically significant differences in the levels of cortical microtubules in *cls-2* oocytes (data not shown). Alternatively, mammalian CLASPs mediate linkage between microtubule plus ends and the cell cortex (53, 54), and such interactions might also influence cortical stiffness in *C. elegans* oocytes. Other factors, including the kinesin-13 family member KLP-7 and the TOG domain protein and XMAP215 ortholog ZYG-9, have been shown to down-regulate cortical microtubule levels during oocyte meiotic cell division in *C. elegans* (21, 55). Further investigation both of microtubule and actomyosin dynamics, using higher resolution light microscopy methods, and studies of how microfilament and microtubule regulators interact to influence oocyte cortical dynamics, may improve our understanding of how global cortical contractility and membrane dynamics influence contractile ring dynamics during polar body extrusion.

Comparing the consequences of reducing the functions of the casein kinase CNSK-1 and CLS-2 indicates that the relationship between global cortical dynamics and polar body extrusion is complex. CSNK-1 also limits membrane ingressions throughout

the oocyte cortex during meiosis I but appears to do so through negative regulation of actomyosin dynamics, and CSNK-1 knockdown often results in extrusion of the entire meiotic spindle and all of the oocyte chromosomes into the first polar body (15). This outcome has led to a model in which global cortical contraction generates a hydrostatic cytoplasmic force that promotes an out-pocketing of the plasma membrane as the spindle is pushed through the contractile ring and into the forming polar body. While such a mechanism may operate, it also is clear that the contractile ring and associated plasma membrane ingress substantially prior to constricting roughly midway along the axis of the spindle during polar body extrusion. These dynamics suggest that the spindle and the contractile ring interact to promote furrow ingression and constriction. Moreover, the increased global membrane ingressions in *cls-2* oocytes do not appear to result from increased actomyosin contractility and are accompanied by defects in ring assembly or stability and a frequent failure to extrude a polar body. Thus, it appears that negative regulation of global cortical membrane ingression during oocyte meiotic cell division can both promote and prevent the extrusion of chromosomes into polar bodies. These different outcomes presumably reflect differences in how CSNK-1 and CLS-2 influence the cortical cytoskeleton and its dynamics. One possible explanation for these different outcomes is that a loss of cortical stiffness in *cls-2* oocytes might allow for increased membrane ingression throughout the oocyte cortex, while at the same time disrupting contractile ring assembly and/or preventing any increase in the hydrostatic cytoplasmic force that has been proposed to push the meiotic spindle partly into the budding polar body (15). Further investigation of cortical cytoskeleton dynamics, and the interactions of factors that regulate these dynamics during polar body extrusion, should

581 improve our understanding of this poorly understood but fundamentally important

582 biological process.

583 **Materials and methods**

584 ***C. elegans* Strain Maintenance**

585 All *C. elegans* strains used in this study (S1 Table), were maintained at 20ºC as

586 described previously (56).

587

588 ***cls-2* CRISPR/Cas9 Allele Generation**

589 Mutations in *cls-2* were generated by injecting young adult N2 hermaphrodites with the

590 following mixture (57): 25μM *cls-2* crRNA (ATCAGCCGATCGACTCCGGG), 5μM *dpy-*

591 *10* crRNA (GCTACCATAGGCACCAC GAG), 30μM trRNA, 2.1μg/μl Cas9-NLS, and

592 2.5μM *dpy-10* single-strand DNA (ssDNA,

593 CACTTGAACTTCAATACGGCAAGATGAGAATGACTGGAAACCGTACCGCATGCGG

594 TGCCTATGGTAGCGGAGCTTCACATGGCTTCAGACCAACAGCCTAT). No

595 homologous repair template was used for *cls-2,* and *cls-2* DNA breaks were allowed to

596 repair randomly. Before injection, the trRNA and crRNAs were mixed and incubated at

597 95ºC for 5 minutes, before cooling at room temperature for 5 minutes. After cooling,

598 Cas9-NLS (QB3-Berkeley MacroLab) was added to the annealed trRNA and crRNAs

599 and allowed to incubate for another 5 minutes at room temperature before the *dpy-10*

600 ssDNA repair template was added. After injection, hermaphrodites were singled out and

601 their broods were screened for *dpy-10* roller or dumpy co-conversion worms, which

602 were allowed to produce broods. Those broods were then evaluated for potential *cls-2*

603 phenotypes (embryonic lethality), and lines identified as potentially carrying mutations to

604 *cls-2* were balanced. PCR amplified fragments were Sanger sequenced to identify the

605 CRISPR/Cas9-induced mutations.

606

607 **Feeding RNAi Knockdown of *mei-1* and *klp-18***

608 RNAi knockdown of *mei-1* and *klp-18* was achieved by plating hypochlorite
609 synchronized L1 larvae onto *E. coli* (HT115) lawns induced to express dsRNA
610 corresponding to *mei-1* or *klp-18 (58)*. Plated worms were either maintained at 20ºC
611 until adults were imaged (*mei-1*) or maintained at 20ºC and upshifted to 26ºC 16 hours
612 prior to imaging (*klp-18*) to ensure robust knockdown, as determined by the formation of
613 monopolar meiotic spindles in both meiosis I and II. The *mei-1* RNAi vector was from
614 the Ahringer RNAi library (59). The *klp-18* RNAi vector was made by amplifying a
615 portion of the *klp-18* coding sequence from isolated N2 genomic DNA (using primers 5'-
616 ACCGGCAGATCTGATATCATCGATGAATTCTCCAACTTTCAA ATGCCACA-3' and 5'-
617 ACGGTATCGATAAGCTTGATATCGAATTCCTTCGATATGGAA GAA AGCGG-3'),
618 which was inserted into the L4440 vector backbone using the NEBuilder HiFi DNA
619 assembly cloning kit (NEB).

620

621 **Live-cell Imaging**

622 All imaging was carried out using a Leica DMi8 microscope outfitted with a spinning disk
623 confocal unit – CSU-W1 (Yokogawa) with Borealis (Andor), dual iXon Ultra 897 (Andor)
624 cameras, and a 100x HCX PL APO 1.4-0.70NA oil objective lens (Leica). Metamorph
625 (Molecular Devices) imaging software was used for controlling image acquisition. The
626 488nm and 561nm channels were imaged simultaneously every 10 seconds with 1μm
627 Z-spacing (either 16μm or 21μm total Z-stacks depending on the fluorescent markers

used, with the same stack size used for all movies utilizing the same fluorescent markers).

In utero live imaging of oocytes was accomplished by mounting adult worms with a single row or less of embryos in 1.5μl of M9 mixed with 1.5μl of 0.1μm polystyrene Microspheres (Polysciences Inc.) on a 6% agarose pad with a coverslip gently laid over top. *Ex utero* imaging of oocytes was carried out by cutting open adult worms with a single row or less of embryos in 4μl of egg buffer (118mM NaCl, 48mM KCl, 2mM $CaCl_2$, 2mM $MgCl_2$, and 0.025 mM of HEPES, filter sterilized before HEPES addition) on a coverslip before mounting onto a 2% agarose pad on a microscope slide.

Image analysis, Quantification, and Statistical Analysis

General image analysis and quantification of microtubules and global cortical furrowing was carried out using FIJI software (60). Three-dimensional projection and rotation of movies used to look at polar body contractile rings was carried out using Imaris software (Bitplane). Meiosis I polar body extrusion success was evaluated based on whether oocytes extruded any chromosomes marked by GFP or mCherry histone 2B (H2B) into a polar body that remained extruded for the period of imaging, either until meiosis I had obviously ended and meiosis II spindle assembly began, or until pronuclei began to decondense in the one-cell stage embryo after meiosis II. The end of meiosis I and beginning of meiosis II was considered to be the time at which the chromosomes left in the oocyte cytoplasm began to visibly separate from each other. Projections for spindle-associated furrow examination were made by manually isolating the 5 most spindle-associated z-planes for each time point during the period of global cortical furrowing and

651 then sum projecting the mCherry::PH membrane signal. Membrane temporal overlays
652 were created by overlaying the outlined membrane regions of interest for the period of
653 furrowing (detailed below) to create a single image.
654 Total spindle microtubule pixel intensity was determined using the following
655 formula: (Mean Grey Value (spindle)/Mean Grey Value (cytoplasm)) × spindle area =
656 total spindle microtubule pixel intensity. The mean grey values for both the meiotic
657 spindle and cytoplasm were determined by drawing a region of interest around either
658 the meiotic spindle or a portion of oocyte cytoplasm devoid of adjacent sperm in
659 maximum projected Z-stacks and measuring the mean grey value of the selected region
660 in ImageJ. Spindle area was determined by measuring the area of the region of interest
661 encompassing the meiotic spindle.
662 Quantification of global cortical furrowing was accomplished by drawing regions
663 of interest over the oocyte membrane signal (mCherry::PH) for a single central z-slice
664 for the entire period of global cortical furrowing. Regions of interest were then converted
665 to a high contrast stack of membrane positions over time, which were then analyzed
666 using the ADAPT plugin (61) for ImageJ in order to determine curvature values across
667 the oocyte membrane. A furrow was defined as being at least two consecutive
668 membrane points with negative mean curvature values and a standard deviation of
669 mean curvature at least two standard deviations above the average standard deviation
670 of mean curvature value for the entire oocyte membrane. Membrane points fitting the
671 criteria of a furrow (above) that were separated by a single membrane point not fitting
672 the criteria were considered as part of the same furrow for the purposes of counting. For
673 statistical analysis of global cortical furrowing (Fig 7B), one-way ANOVA was used to

674 determine if there was any difference in the mean furrowing between genotypes, F-
675 Tests to compare the variances, and two-tailed Student's t-Tests between genotypes to
676 compare the means directly (assuming either equal or unequal variances depending on
677 the F-Test results). Statistical analysis and graphs were completed using Excel
678 (Microsoft).
679

680 **Acknowledgements**

681 We thank Julien Dumont, Amy Maddox, and the Caenorhabditis Genetics Center
682 (funded by the NIH Office of Research Infrastructure Programs; P40 OD010440) for *C.*
683 *elegans* strains, Jie Yang for the KLP-18 RNAi vector, Chris Doe and Diana Libuda for
684 sharing laboratory equipment, and members of the Bowerman laboratory for helpful
685 discussions.
686

687 **Figure Legends**

688 **Fig 1 – Schematics of oocyte meiotic polar body extrusion, mitotic cytokinesis**
689 **and oocyte meiotic spindle assembly-defective mutants.** (A) The positioning and
690 dynamics of contractile ring assembly and ingression during oocyte polar body extrusion
691 and mitotic cytokinesis. (B) Illustrations of oocyte meiotic spindle structure in control and
692 mutant oocytes. Green = microtubules, blue = chromosomes, magenta = contractile
693 rings, and orange = ASPM-1 pole marker, black = plasma membrane. See text for
694 details.
695

Fig 2 – CLS-2 is required for oocyte meiotic spindle assembly and polar body extrusion. (A) Control oocytes expressing CLS-2::GFP and mCherry:H2B during meiosis I; dashed boxes indicate the zoomed-in regions shown in top row. (B) Protein domain map for wild type CLS-2 (28), and location of first premature stop codon due to frameshift in *cls-2(or1948)*. (C) Table of embryonic viability in wild type (N2) and *cls-2* CRISPR-generated loss of function alleles. (D) *C*ontrol and mutant oocytes expressing GFP::Tubulin and mCherry::H2B during meiosis I; t = 0 seconds (0s) corresponds to the end of meiosis I and beginning of meiosis II (see Materials and methods). (E) Comparison of integrated spindle microtubule pixel intensity over time between control (n = 17) and *cls-2* mutant oocytes (n = 9 @ -340s, n = 10 @ -330 to -300s, n = 11 @ -290 to -160s, and n = 12 @ -150 to 0s), with the average intensity indicated and one standard deviation indicated. Here and in subsequent figure panels, T = 0s corresponds to the end of meiosis I and beginning of meiosis II, unless indicated otherwise (see Materials and methods). (F) *C*ontrol and mutant oocytes expressing GFP::ASPM-1 and mCherry::H2B during meiosis I. (G) Percent of control and mutant oocytes that extrude a polar body during meiosis I, as determined by mCherry or GFP-fused histone signal remaining stably ejected from the oocyte cytoplasm for the duration of imaging (see Materials and methods).

Fig 3 – Central spindle proteins AIR-2 and CYK-4 still associate with spindle microtubules in *cls-2* mutant oocytes. Control and *cls-2* mutant oocytes expressing GFP::AIR-2 and mCherry::H2B (A) or GFP::CYK-4 and mCherry::H2B (B) during meiosis I.

719

720 **Fig 4 – Spindle-associated membrane furrowing during meiosis I in control and**
721 **mutant oocytes.** Images show projections of five focal planes encompassing the
722 chromosomes during meiosis I in oocytes expressing an mCherry fusion to a PH
723 domain to mark the plasma membrane using sum projections and GFP::H2B using
724 maximum projections. Representative examples of control (A, B), *cls-2* mutant (C-E),
725 *klp-18(RNAi)* (F, G) and *mei-1(RNAi)* (H, I) oocytes. Polar body extrusion failed in C-E
726 and H, and was successful in all others. T = 0s corresponds to the timepoint
727 immediately before cortical furrowing begins. See text for details.

728

729 **Fig 5 – Contractile ring non-muscle myosin NMY-2 dynamics during meiosis I in**
730 **control and mutant oocytes.** Three-dimensionally projected and rotated images of
731 control (A), *cls-2* mutant (B), *klp-18(RNAi)* (C), and *mei-1(RNAi)* (D) oocytes expressing
732 NMY-2::GFP and mCherry::H2B. Z-stacks were rotated as to look down on contractile
733 ring assembly and dynamics over time.

734

735 **Fig 6 – Contractile ring anillin ANI-1 and non-muscle myosin NMY-2 dynamics**
736 **during meiosis I in control and *cls-2* mutant oocytes.** Three-dimensionally projected
737 and rotated images of control and *cls-2* mutant oocytes expressing mNeonGreen::ANI-1
738 and mCherry::H2B (A) or NMY-2::mKate2, mNeonGreen::ANI-1, and mCherry::H2B,
739 with overlays shown in top row for each set. Z-stacks were rotated so as to look down
740 on contractile ring assembly and dynamics over time.

741

Fig 7 – Membrane ingressions throughout the oocyte cortex during meiosis I in control and mutant oocytes. (A) Membrane temporal overlays for control, *cls-2* mutant, *klp-18(RNAi)*, and *mei-1(RNAi)* oocytes representing the membrane positions of a single focal plane during the period of meiosis I global cortical furrowing for a single oocyte of each genotype. (B) Quantification of the number of global cortical furrows in control and mutant oocytes (see Materials and methods). t-Test results: Control vs *cls-2(or1948)* p = 0.0014 (**), *cls-2(or1948)* vs *klp-18(RNAi)* p = 3.14E-5 (***), *cls-2(or1948)* vs *mei-1(RNAi)* p = 0.054 (ns). (C and D) *C*ontrol and *cls-2* mutant oocytes expressing (C) NMY-2::GFP and mCherry::H2B or (D) mNeonGreen::ANI-1 and mCherry::H2B.

S1 Fig - CLS-2 localizes to meiotic spindles and is required for their assembly (A) *In utero* time-lapse spinning disk confocal images of CLS-2::GFP and mCherry::H2B. (B) Protein domain maps of wild type CLS-2 and CRISPR-generated *cls-2* alleles *or1949*, *or1950*, and *or1951*. Each mutation results in multiple early stop codons before the first TOG domain, with the first stop codon indicated. (C) *In utero* time-lapse spinning disk confocal images of control and *cls-2* mutant oocytes with GFP::TBB-2 and mCherry::H2B. t = 0 seconds corresponds to nuclear envelope breakdown.

S2 Fig - Control oocyte spindle-associated membrane furrows Time-lapse spinning disk confocal images of control oocytes expressing mCherry::PH and GFP::H2B; t = 0 seconds here and in subsequent Fig 4 related supplements (S3-6

764 Figs) corresponds to the time point immediately before global cortical furrowing begins,
765 unless otherwise stated.
766
767 **S3 Fig - *cls-2(or1948)* oocyte spindle-associated membrane furrows**
768 Time-lapse spinning disk confocal images of *cls-2* mutant oocytes expressing
769 mCherry::PH and GFP::H2B.
770
771 **S4 Fig - *cls-2(or1948)* oocyte spindle-associated membrane furrows**
772 Time-lapse spinning disk confocal images of *cls-2* mutant oocytes expressing
773 mCherry::PH and GFP::H2B.
774
775 **S5 Fig – *klp-18(RNAi)* oocyte spindle-associated membrane furrows**
776 Time-lapse spinning disk confocal images of *klp-18(RNAi)* oocytes expressing
777 mCherry::PH and GFP::H2B.
778
779 **S6 Fig – *mei-1(RNAi)* oocyte spindle-associated membrane furrows**
780 Time-lapse spinning disk confocal images of *mei-1(RNAi)* oocytes expressing
781 mCherry::PH and GFP::H2B.
782
783 **S7 Fig – Control oocyte NMY-2::GFP contractile rings**
784 Three-dimensionally projected and rotated spinning disk confocal time-lapse images of
785 control oocytes expressing NMY-2::GFP and mCherry::H2B; t = 0 seconds in this and

786 subsequent Fig 5 related supplements (S8-10 Figs) corresponds to the end of meiosis I
787 and beginning of meiosis II (see Materials and methods).
788
789 **S8 Fig – *cls-2(or1948)* oocyte NMY-2::GFP contractile rings**
790 Three-dimensionally projected and rotated spinning disk confocal time-lapse images of
791 *cls-2* mutant oocytes expressing NMY-2::GFP and mCherry::H2B.
792
793 **S9 Fig – *klp-18(RNAi)* oocyte NMY-2::GFP contractile rings**
794 Three-dimensionally projected and rotated spinning disk confocal time-lapse images of
795 *klp-18(RNAi)* oocytes expressing NMY-2::GFP and mCherry::H2B.
796
797 **S10 Fig – *mei-1(RNAi)* oocyte NMY-2::GFP contractile rings**
798 Three-dimensionally projected and rotated spinning disk confocal time-lapse images of
799 *mei-1(RNAi)* oocytes expressing NMY-2::GFP and mCherry::H2B.
800
801 **S11 Fig – Control oocyte membrane temporal overlays**
802 Control oocyte membrane temporal overlays depicting membrane positions over time at
803 a single focal plane throughout meiosis I.
804
805 **S12 Fig – *cls-2(or1948)* oocyte membrane temporal overlays**
806 *cls-2* mutant oocyte membrane temporal overlays depicting membrane positions over
807 time at a single focal plane throughout meiosis I. Asterisks indicate oocytes in which
808 polar body extrusion failed.

S13 Fig – *klp-18(RNAi)* and *mei-1(RNAi)* membrane temporal overlays

klp-18(RNAi) and mei-1(RNAi) oocyte membrane temporal overlays depicting membrane positions over time at a single focal plane throughout meiosis I. Asterisks indicate oocytes in which polar body extrusion failed.

S14 Fig – Control oocyte NMY-2::GFP cortical dynamics

Time-lapse spinning disk confocal images of control oocytes expressing NMY-2::GFP and mCherry:H2B; t = 0 seconds corresponds to the end of meiosis I and beginning of meiosis II in this and subsequent Fig 7 related supplements (S15-18 Figs).

S15 Fig – Control oocyte mNG::ANI-1 cortical dynamics

Time-lapse spinning disk confocal images of control oocytes expressing mNeonGreen::ANI-1 and mCherry::H2B.

S16 Fig – *cls-2(or1948)* oocyte NMY-2::GFP cortical dynamics

Time-lapse spinning disk confocal images of *cls-2* mutant oocytes expressing NMY-2::GFP and mCherry::H2B. All oocytes shown succeeded in polar body extrusion.

S17 Fig – *cls-2(or1948)* oocyte NMY-2::GFP cortical dynamics

Time-lapse spinning disk confocal images of *cls-2* mutant oocytes expressing NMY-2::GFP and mCherry::H2B. All oocytes shown failed in polar body extrusion.

S18 Fig – *cls-2(or1948)* oocyte mNG::ANI-1 cortical dynamics

Time-lapse spinning disk confocal images of *cls-2* mutant oocytes expressing mNeonGreen::ANI-1 and mCherry::H2B; t = 0s corresponds to the end of meiosis I and beginning of meiosis II. All oocytes shown failed in polar body extrusion.

S1 Movie – *Ex utero* CLS-2::GFP localization

Ex utero time-lapse spinning disk confocal movie of a maximum projected oocyte expressing CLS-2::GFP (green) and mCherry::H2B (magenta). Frame rate is 10 frames per second.

S2 Movie – *In utero* CLS-2::GFP localization

In utero time-lapse spinning disk confocal movie of a maximum projected oocyte expressing CLS-2::GFP (green) and mCherry::H2B (magenta). Frame rate is 10 frames per second.

S3 Movie – Control oocyte membrane furrowing

Ex utero time-lapse spinning disk confocal movie of a control oocyte expressing mCherry::PH (black) and GFP::H2B (magenta). In this and subsequent oocyte membrane furrowing videos, the 5 focal planes that encompassed most of the meiotic chromosomes were used; membrane images were sum projected, histones images were maximum projected. In this and all subsequent Fig 4 related movies (S4-10 Movies), the frame rate is 5 frames per second.

S4 Movie – Control oocyte membrane furrowing

Ex utero time-lapse spinning disk confocal movie of a control oocyte expressing mCherry::PH (black) and GFP::H2B (magenta).

S5 Movie – *cls-2(or1948)* oocyte membrane furrowing

Ex utero time-lapse spinning disk confocal movie of a *cls-2(or1948)* oocyte expressing mCherry::PH (black) and GFP::H2B (magenta).

S6 Movie – *cls-2(or1948)* oocyte membrane furrowing

Ex utero time-lapse spinning disk confocal movie of a *cls-2(or1948)* oocyte expressing mCherry::PH (black) and GFP::H2B (magenta).

S7 Movie – *klp-18(RNAi)* oocyte membrane furrowing

Ex utero time-lapse spinning disk confocal movie of a *klp-18(RNAi)* oocyte expressing mCherry::PH (black) and GFP::H2B (magenta).

S8 Movie – *klp-18(RNAi)* oocyte membrane furrowing

Ex utero time-lapse spinning disk confocal movie of a *klp-18(RNAi)* oocyte expressing mCherry::PH (black) and GFP::H2B (magenta).

S9 Movie – *mei-1(RNAi)* oocyte membrane furrowing

Ex utero time-lapse spinning disk confocal movie of a *mei-1(RNAi)* oocyte expressing mCherry::PH (black) and GFP::H2B (magenta).

878

879 **S10 Movie – *mei-1(RNAi)* oocyte membrane furrowing**

880 *Ex utero* time-lapse spinning disk confocal movie of a *mei-1(RNAi)* oocyte expressing

881 mCherry::PH (black) and GFP::H2B (magenta).

882

883 **S11 Movie – Control oocyte NMY-2::GFP contractile ring dynamics**

884 *Ex utero* 3-dimensionally projected and rotated time-lapse spinning disk confocal movie

885 of control oocyte expressing NMY-2::GFP (green) and mCherry:H2B (magenta). In this

886 and all subsequent Fig 5 related movies (S12-18 Movies), the frame rate is 5 frames per

887 second.

888

889 **S12 Movie – Control oocyte NMY-2::GFP contractile ring dynamics**

890 *Ex utero* 3-dimensionally projected and rotated time-lapse spinning disk confocal movie

891 of control oocyte expressing NMY-2::GFP (green) and mCherry:H2B (magenta).

892

893 **S13 Movie – *cls-2(or1948)* oocyte NMY-2::GFP contractile ring dynamics**

894 *Ex utero* 3-dimensionally projected and rotated time-lapse spinning disk confocal movie

895 of *cls-2(or1948)* oocyte expressing NMY-2::GFP (green) and mCherry:H2B (magenta).

896

897 **S14 Movie – *cls-2(or1948)* oocyte NMY-2::GFP contractile ring dynamics**

898 *Ex utero* 3-dimensionally projected and rotated time-lapse spinning disk confocal movie

899 of *cls-2(or1948)* oocyte expressing NMY-2::GFP (green) and mCherry:H2B (magenta).

900

S15 Movie – *klp-18(RNAi)* oocyte NMY-2::GFP contractile ring dynamics

Ex utero 3-dimensionally projected and rotated time-lapse spinning disk confocal movie of *klp-18(RNAi)* oocyte expressing NMY-2::GFP (green) and mCherry:H2B (magenta).

S16 Movie – *klp-18(RNAi)* oocyte NMY-2::GFP contractile ring dynamics

Ex utero 3-dimensionally projected and rotated time-lapse spinning disk confocal movie of *klp-18(RNAi)* oocyte expressing NMY-2::GFP (green) and mCherry:H2B (magenta).

S17 Movie – *mei-1(RNAi)* oocyte NMY-2::GFP contractile ring dynamics

Ex utero 3-dimensionally projected and rotated time-lapse spinning disk confocal movie of *mei-1(RNAi)* oocyte expressing NMY-2::GFP (green) and mCherry:H2B (magenta).

S18 Movie – *mei-1(RNAi)* oocyte NMY-2::GFP contractile ring dynamics

Ex utero 3-dimensionally projected and rotated time-lapse spinning disk confocal movie of *mei-1(RNAi)* oocyte expressing NMY-2::GFP (green) and mCherry:H2B (magenta).

S19 Movie – Control oocyte mNG::ANI-1 contractile ring dynamics

Ex utero 3-dimensionally projected and rotated time-lapse spinning disk confocal movie of control oocyte expressing mNG::ANI-1 (green) and mCherry:H2B (magenta). In this and all subsequent Fig 6 related movies (S20-22 Movies), the frame rate is 5 frames per second.

S20 Movie – *cls-2(or1948)* oocyte mNG::ANI-1 contractile ring dynamics

924 *Ex utero* 3-dimensionally projected and rotated time-lapse spinning disk confocal movie
925 of *cls-2(or1948)* oocyte expressing mNG::ANI-1 (green) and mCherry:H2B (magenta).
926
927 **S21 Movie – Control oocyte NMY-2::mKate2 and mNG::ANI-1 contractile ring**
928 **dynamics**
929 *Ex utero* 3-dimensionally projected and rotated time-lapse spinning disk confocal movie
930 of control oocyte expressing NMY-2::mKate2 (magenta), mNG::ANI-1 (green), and
931 mCherry:H2B (magenta).
932
933 **S22 Movie – *cls-2(or1948)* oocyte NMY-2::mKate2 and mNG::ANI-1 contractile ring**
934 **dynamics**
935 *Ex utero* 3-dimensionally projected and rotated time-lapse spinning disk confocal movie
936 of *cls-2(or1948)* oocyte expressing NMY-2::mKate2 (magenta), mNG::ANI-1 (green),
937 and mCherry:H2B (magenta).
938
939 **S23 Movie – Control oocyte NMY-2::GFP cortical dynamics**
940 Three example time-lapse spinning disk confocal movies of *ex utero* control oocytes
941 expressing NMY-2::GFP (green) and mCherry::H2B (magenta). In this and all
942 subsequent Fig 7 related movies (S24-26 Movies), the frame rate is 5 frames per
943 second.
944
945 **S24 Movie – *cls-2(or1948)* oocyte NMY-2::GFP cortical dynamics**

946 Three example time-lapse spinning disk confocal movies of *ex utero cls-2(or1948)*
947 oocytes expressing NMY-2::GFP (green) and mCherry::H2B (magenta).
948
949 **S25 Movie – Control oocyte mNG::ANI-1 cortical dynamics**
950 Three example time-lapse spinning disk confocal movies of *ex utero* control oocytes
951 expressing mNG::ANI-1 (green) and mCherry::H2B (magenta).
952
953 **S26 Movie – *cls-2(or1948)* oocyte mNG::ANI-1 cortical dynamics**
954 Three example time-lapse spinning disk confocal movies of *ex utero cls-2(or1948)*
955 oocytes expressing mNG::ANI-1 (green) and mCherry::H2B (magenta).
956
957 **S1 Table – Table of *C. elegans* strains used in this study**
958

References

1. Dumont J, Desai A. Acentrosomal spindle assembly and chromosome segregation during oocyte meiosis. Trends Cell Biol. 2012;22(5):241-9.

2. Severson AF, von Dassow G, Bowerman B. Oocyte Meiotic Spindle Assembly and Function. Curr Top Dev Biol. 2016;116:65-98.

3. Mullen TJ, Davis-Roca AC, Wignall SM. Spindle assembly and chromosome dynamics during oocyte meiosis. Curr Opin Cell Biol. 2019;60:53-9.

4. Ohkura H. Meiosis: an overview of key differences from mitosis. Cold Spring Harb Perspect Biol. 2015;7(5).

5. Maddox AS, Azoury J, Dumont J. Polar body cytokinesis. Cytoskeleton (Hoboken). 2012;69(11):855-68.

6. Pintard L, Bowerman B. Mitotic Cell Division in *Caenorhabditis elegans*. Genetics. 2019;211(1):35-73.

7. Green RA, Paluch E, Oegema K. Cytokinesis in animal cells. Annu Rev Cell Dev Biol. 2012;28:29-58.

8. Basant A, Glotzer M. Spatiotemporal Regulation of RhoA during Cytokinesis. Curr Biol. 2018;28(9):R570-R80.

9. Shelton CA, Carter JC, Ellis GC, Bowerman B. The nonmuscle myosin regulatory light chain gene mlc-4 is required for cytokinesis, anterior-posterior polarity, and body morphology during Caenorhabditis elegans embryogenesis. J Cell Biol. 1999;146(2):439-51.

10. Fabritius AS, Flynn JR, McNally FJ. Initial diameter of the polar body contractile ring is minimized by the centralspindlin complex. Dev Biol. 2011;359(1):137-48.

11. Swan KA, Severson AF, Carter JC, Martin PR, Schnabel H, Schnabel R, et al. cyk-1: a C. elegans FH gene required for a late step in embryonic cytokinesis. J Cell Sci. 1998;111 (Pt 14):2017-27.

12. Dorn JF, Zhang L, Paradis V, Edoh-Bedi D, Jusu S, Maddox PS, et al. Actomyosin tube formation in polar body cytokinesis requires Anillin in C. elegans. Curr Biol. 2010;20(22):2046-51.

13. Schonegg S, Hyman AA. CDC-42 and RHO-1 coordinate acto-myosin contractility and PAR protein localization during polarity establishment in C. elegans embryos. Development. 2006;133(18):3507-16.

14. Schumacher JM, Golden A, Donovan PJ. AIR-2: An Aurora/Ipl1-related protein kinase associated with chromosomes and midbody microtubules is required for polar body extrusion and cytokinesis in Caenorhabditis elegans embryos. J Cell Biol. 1998;143(6):1635-46.

15. Flynn JR, McNally FJ. A casein kinase 1 prevents expulsion of the oocyte meiotic spindle into a polar body by regulating cortical contractility. Mol Biol Cell. 2017;28(18):2410-9.

16. Clandinin TR, Mains PE. Genetic studies of mei-1 gene activity during the transition from meiosis to mitosis in Caenorhabditis elegans. Genetics. 1993;134(1):199-210.

17. Mains PE, Kemphues KJ, Sprunger SA, Sulston IA, Wood WB. Mutations affecting the meiotic and mitotic divisions of the early Caenorhabditis elegans embryo. Genetics. 1990;126(3):593-605.

18. Deng M, Li R. Sperm chromatin-induced ectopic polar body extrusion in mouse eggs after ICSI and delayed egg activation. PLoS One. 2009;4(9):e7171.

19. Deng M, Suraneni P, Schultz RM, Li R. The Ran GTPase mediates chromatin signaling to control cortical polarity during polar body extrusion in mouse oocytes. Dev Cell. 2007;12(2):301-8.

20. Askjaer P, Galy V, Hannak E, Mattaj IW. Ran GTPase cycle and importins alpha and beta are essential for spindle formation and nuclear envelope assembly in living Caenorhabditis elegans embryos. Mol Biol Cell. 2002;13(12):4355-70.

21. Chuang C-H, Schlientz AJ, Yang J, Bowerman B. Microtubule Assembly and Pole Coalescence: Early Steps in *C. elegans* Oocyte Meiosis I Spindle Assembly. BioRxiv. 2020.

22. Byrnes AE, Slep KC. TOG-tubulin binding specificity promotes microtubule dynamics and mitotic spindle formation. J Cell Biol. 2017;216(6):1641-57.

1018 23. Patel K, Nogales E, Heald R. Multiple domains of human CLASP contribute to
1019 microtubule dynamics and organization in vitro and in Xenopus egg extracts.
1020 Cytoskeleton (Hoboken). 2012;69(3):155-65.
1021 24. Al-Bassam J, Kim H, Brouhard G, van Oijen A, Harrison SC, Chang F. CLASP
1022 promotes microtubule rescue by recruiting tubulin dimers to the microtubule. Dev Cell.
1023 2010;19(2):245-58.
1024 25. Aher A, Kok M, Sharma A, Rai A, Olieric N, Rodriguez-Garcia R, et al. CLASP
1025 Suppresses Microtubule Catastrophes through a Single TOG Domain. Dev Cell.
1026 2018;46(1):40-58 e8.
1027 26. Tsvetkov AS, Samsonov A, Akhmanova A, Galjart N, Popov SV. Microtubule-
1028 binding proteins CLASP1 and CLASP2 interact with actin filaments. Cell Motil
1029 Cytoskeleton. 2007;64(7):519-30.
1030 27. Dumont J, Oegema K, Desai A. A kinetochore-independent mechanism drives
1031 anaphase chromosome separation during acentrosomal meiosis. Nat Cell Biol.
1032 2010;12(9):894-901.
1033 28. Maton G, Edwards F, Lacroix B, Stefanutti M, Laband K, Lieury T, et al.
1034 Kinetochore components are required for central spindle assembly. Nat Cell Biol.
1035 2015;17(7):953.
1036 29. Espiritu EB, Krueger LE, Ye A, Rose LS. CLASPs function redundantly to
1037 regulate astral microtubules in the C. elegans embryo. Dev Biol. 2012;368(2):242-54.
1038 30. Pelisch F, Bel Borja L, Jaffray EG, Hay RT. Sumoylation regulates protein
1039 dynamics during meiotic chromosome segregation in. J Cell Sci. 2019;132(14).
1040 31. Tanenbaum ME, Macůrek L, Janssen A, Geers EF, Alvarez-Fernández M,
1041 Medema RH. Kif15 cooperates with eg5 to promote bipolar spindle assembly. Curr Biol.
1042 2009;19(20):1703-11.
1043 32. Sturgill EG, Ohi R. Kinesin-12 differentially affects spindle assembly depending
1044 on its microtubule substrate. Curr Biol. 2013;23(14):1280-90.
1045 33. Vanneste D, Takagi M, Imamoto N, Vernos I. The role of Hklp2 in the
1046 stabilization and maintenance of spindle bipolarity. Curr Biol. 2009;19(20):1712-7.
1047 34. Connolly AA, Osterberg V, Christensen S, Price M, Lu C, Chicas-Cruz K, et al.
1048 Caenorhabditis elegans oocyte meiotic spindle pole assembly requires microtubule

severing and the calponin homology domain protein ASPM-1. Mol Biol Cell. 2014;25(8):1298-311.

35. Wignall SM, Villeneuve AM. Lateral microtubule bundles promote chromosome alignment during acentrosomal oocyte meiosis. Nat Cell Biol. 2009;11(7):839-44.

36. Wolff ID, Tran MV, Mullen TJ, Villeneuve AM, Wignall SM. Assembly of Caenorhabditis elegans acentrosomal spindles occurs without evident microtubule-organizing centers and requires microtubule sorting by KLP-18/kinesin-12 and MESP-1. Mol Biol Cell. 2016;27(20):3122-31.

37. Clark-Maguire S, Mains PE. mei-1, a gene required for meiotic spindle formation in Caenorhabditis elegans, is a member of a family of ATPases. Genetics. 1994;136(2):533-46.

38. Srayko M, Buster DW, Bazirgan OA, McNally FJ, Mains PE. MEI-1/MEI-2 katanin-like microtubule severing activity is required for Caenorhabditis elegans meiosis. Genes Dev. 2000;14(9):1072-84.

39. McNally K, Berg E, Cortes DB, Hernandez V, Mains PE, McNally FJ. Katanin maintains meiotic metaphase chromosome alignment and spindle structure in vivo and has multiple effects on microtubules in vitro. Mol Biol Cell. 2014;25(7):1037-49.

40. Joly N, Martino L, Gigant E, Dumont J, Pintard L. Microtubule-severing activity of the AAA+ ATPase Katanin is essential for female meiotic spindle assembly. Development. 2016;143(19):3604-14.

41. Laband K, Le Borgne R, Edwards F, Stefanutti M, Canman JC, Verbavatz JM, et al. Chromosome segregation occurs by microtubule pushing in oocytes. Nat Commun. 2017;8(1):1499.

42. Han X, Gomes JE, Birmingham CL, Pintard L, Sugimoto A, Mains PE. The role of protein phosphatase 4 in regulating microtubule severing in the Caenorhabditis elegans embryo. Genetics. 2009;181(3):933-43.

43. Gomes JE, Tavernier N, Richaudeau B, Formstecher E, Boulin T, Mains PE, et al. Microtubule severing by the katanin complex is activated by PPFR-1-dependent MEI-1 dephosphorylation. J Cell Biol. 2013;202(3):431-9.

1078 44. Connolly AA, Sugioka K, Chuang CH, Lowry JB, Bowerman B. KLP-7 acts
1079 through the Ndc80 complex to limit pole number in C. elegans oocyte meiotic spindle
1080 assembly. J Cell Biol. 2015;210(6):917-32.
1081 45. Davis-Roca AC, Muscat CC, Wignall SM. oocytes detect meiotic errors in the
1082 absence of canonical end-on kinetochore attachments. J Cell Biol. 2017;216(5):1243-
1083 53.
1084 46. Piekny AJ, Maddox AS. The myriad roles of Anillin during cytokinesis. Semin Cell
1085 Dev Biol. 2010;21(9):881-91.
1086 47. Srayko M, O'toole ET, Hyman AA, Müller-Reichert T. Katanin disrupts the
1087 microtubule lattice and increases polymer number in C. elegans meiosis. Curr Biol.
1088 2006;16(19):1944-9.
1089 48. Inoue YH, Savoian MS, Suzuki T, Máthé E, Yamamoto MT, Glover DM.
1090 Mutations in orbit/mast reveal that the central spindle is comprised of two microtubule
1091 populations, those that initiate cleavage and those that propagate furrow ingression. J
1092 Cell Biol. 2004;166(1):49-60.
1093 49. Crowder ME, Flynn JR, McNally KP, Cortes DB, Price KL, Kuehnert PA, et al.
1094 Dynactin-dependent cortical dynein and spherical spindle shape correlate temporally
1095 with meiotic spindle rotation in Caenorhabditis elegans. Mol Biol Cell.
1096 2015;26(17):3030-46.
1097 50. Hagmann J, Burger MM, Dagan D. Regulation of plasma membrane blebbing by
1098 the cytoskeleton. J Cell Biochem. 1999;73(4):488-99.
1099 51. Sugiyama T, Pramanik MK, Yumura S. Microtubule-Mediated Inositol Lipid
1100 Signaling Plays Critical Roles in Regulation of Blebbing. PLoS One.
1101 2015;10(8):e0137032.
1102 52. Tinevez JY, Schulze U, Salbreux G, Roensch J, Joanny JF, Paluch E. Role of
1103 cortical tension in bleb growth. Proc Natl Acad Sci U S A. 2009;106(44):18581-6.
1104 53. Mimori-Kiyosue Y, Grigoriev I, Lansbergen G, Sasaki H, Matsui C, Severin F, et
1105 al. CLASP1 and CLASP2 bind to EB1 and regulate microtubule plus-end dynamics at
1106 the cell cortex. J Cell Biol. 2005;168(1):141-53.

54. Lansbergen G, Grigoriev I, Mimori-Kiyosue Y, Ohtsuka T, Higa S, Kitajima I, et al. CLASPs attach microtubule plus ends to the cell cortex through a complex with LL5beta. Dev Cell. 2006;11(1):21-32.

55. Gigant E, Stefanutti M, Laband K, Gluszek-Kustusz A, Edwards F, Lacroix B, et al. Inhibition of ectopic microtubule assembly by the kinesin-13 KLP-7 prevents chromosome segregation and cytokinesis defects in oocytes. Development. 2017;144(9):1674-86.

56. Brenner S. The genetics of Caenorhabditis elegans. Genetics. 1974;77(1):71-94.

57. Paix A, Folkmann A, Rasoloson D, Seydoux G. High Efficiency, Homology-Directed Genome Editing in Caenorhabditis elegans Using CRISPR-Cas9 Ribonucleoprotein Complexes. Genetics. 2015;201(1):47-54.

58. Kamath RS, Martinez-Campos M, Zipperlen P, Fraser AG, Ahringer J. Effectiveness of specific RNA-mediated interference through ingested double-stranded RNA in Caenorhabditis elegans. Genome Biol. 2001;2(1):RESEARCH0002.

59. Fraser AG, Kamath RS, Zipperlen P, Martinez-Campos M, Sohrmann M, Ahringer J. Functional genomic analysis of C. elegans chromosome I by systematic RNA interference. Nature. 2000;408(6810):325-30.

60. Schindelin J, Arganda-Carreras I, Frise E, Kaynig V, Longair M, Pietzsch T, et al. Fiji: an open-source platform for biological-image analysis. Nat Methods. 2012;9(7):676-82.

61. Barry DJ, Durkin CH, Abella JV, Way M. Open source software for quantification of cell migration, protrusions, and fluorescence intensities. J Cell Biol. 2015;209(1):163-80.

Fig 1

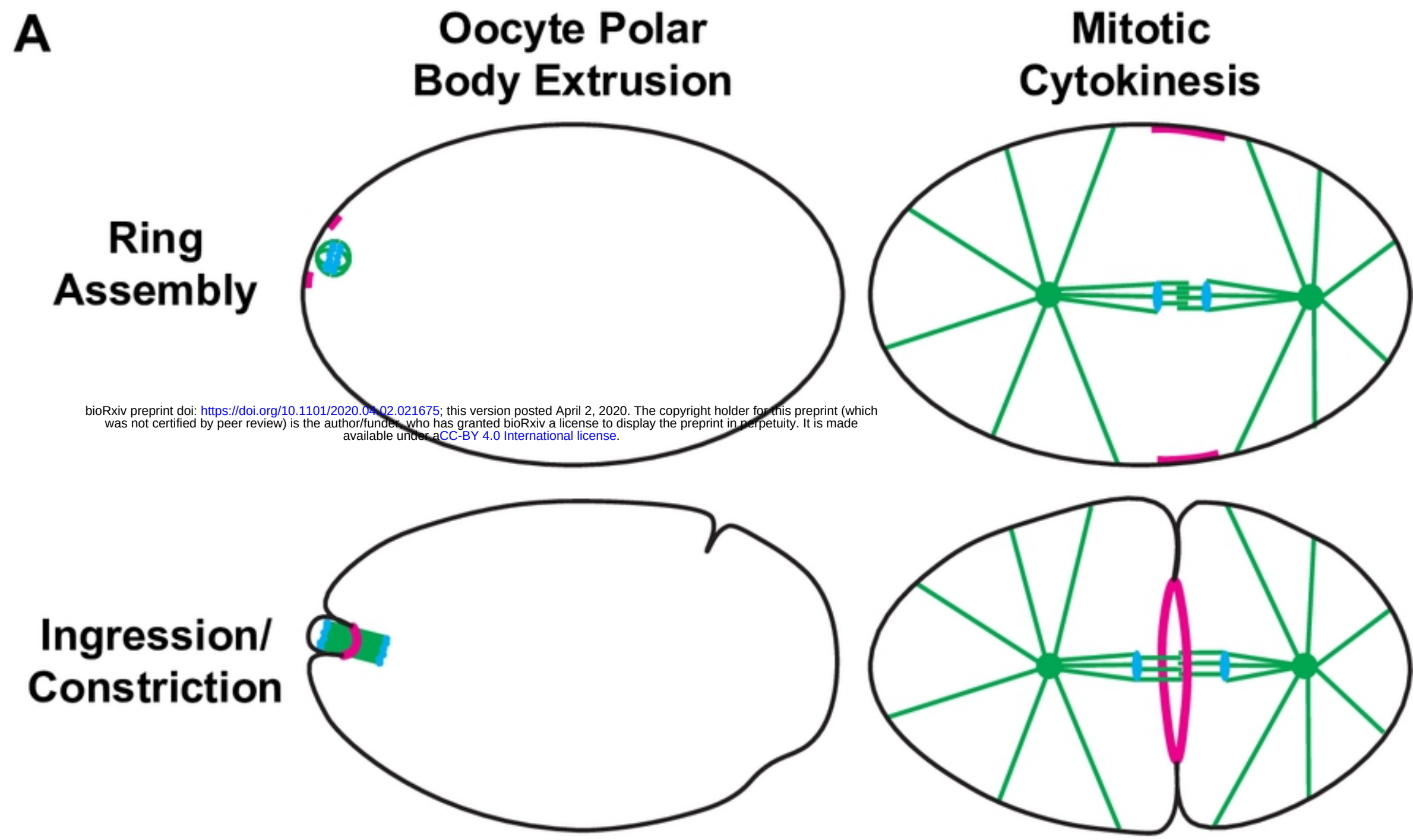

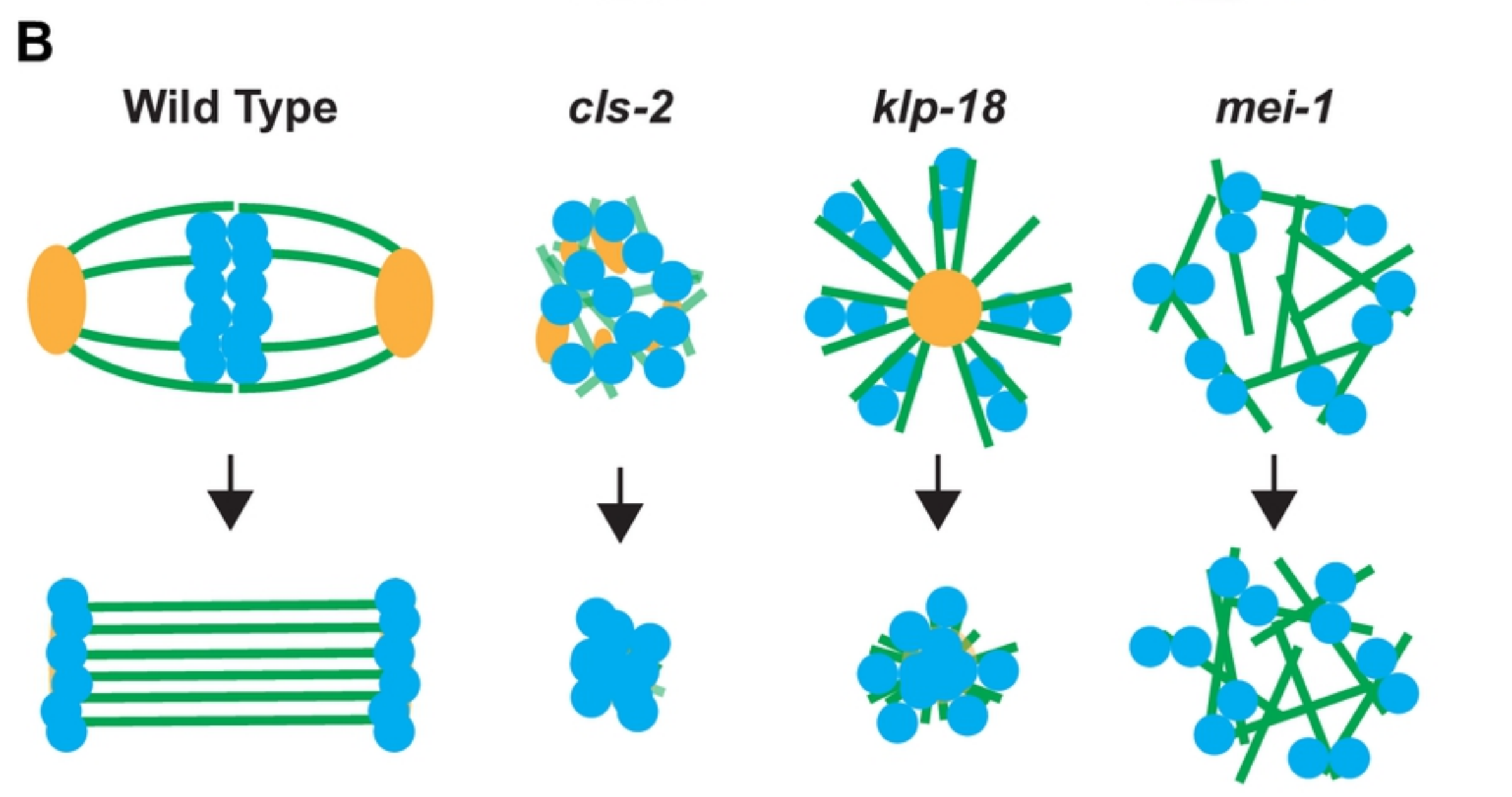

Fig 1

Fig 2

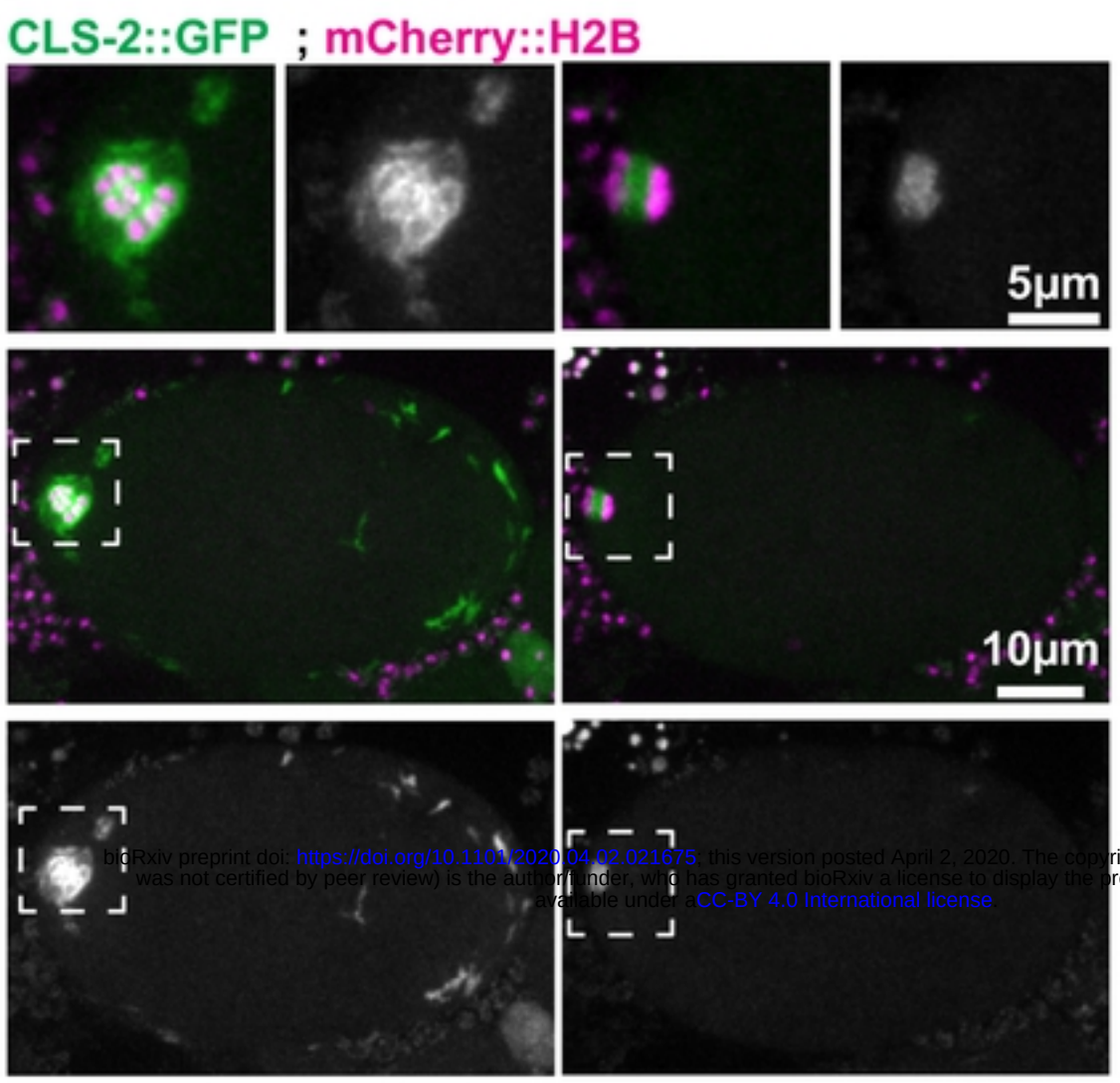

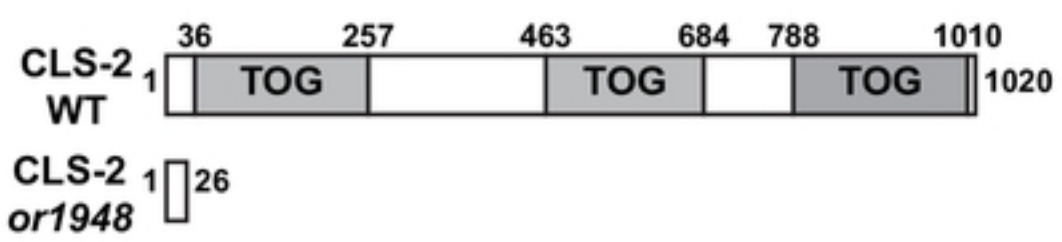

C

Allele	Embryonic Viability (%)
Wild Type	99 (n=844)
cls-2(or1948)	0 (n=375)
cls-2(or1949)	0 (n=436)
cls-2(or1950)	0 (n=1314)
cls-2(or1951)	0 (n=724)

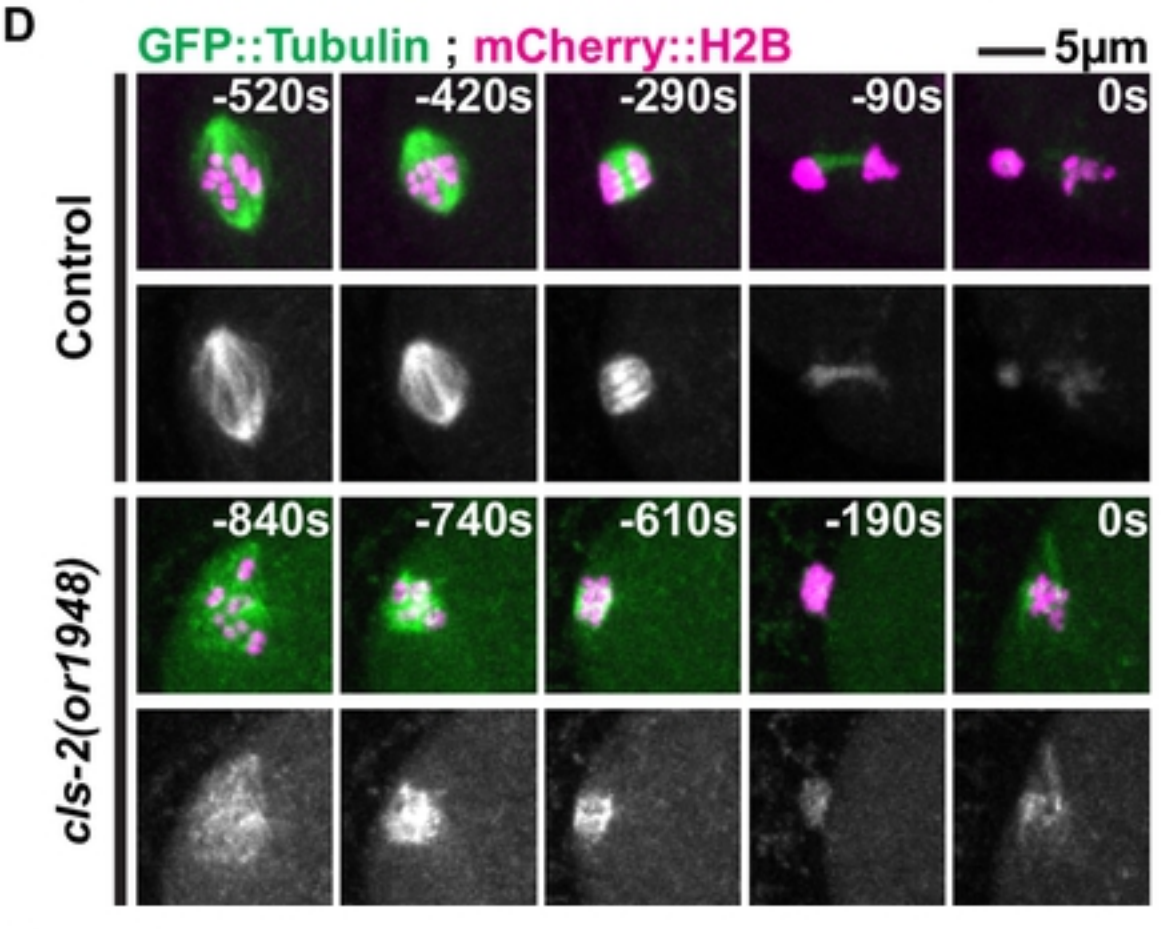

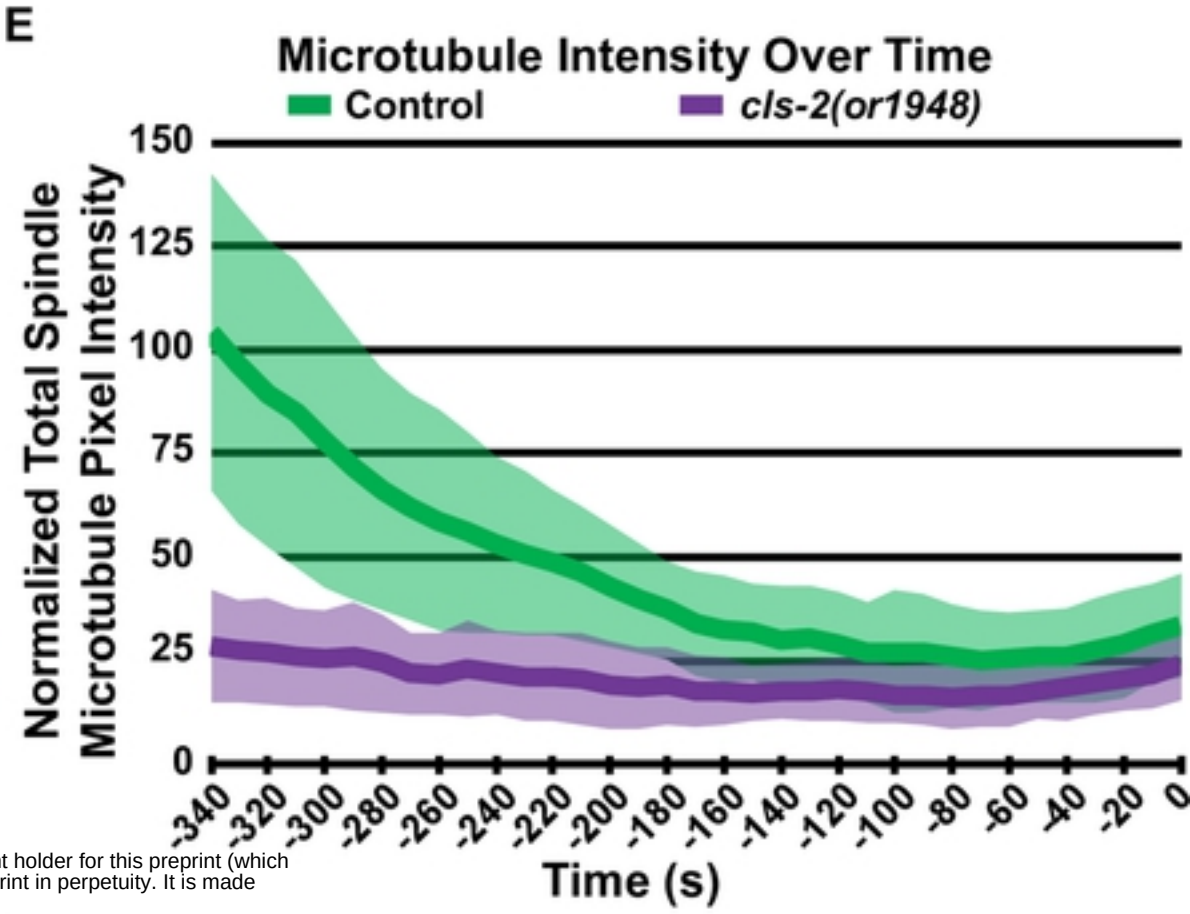

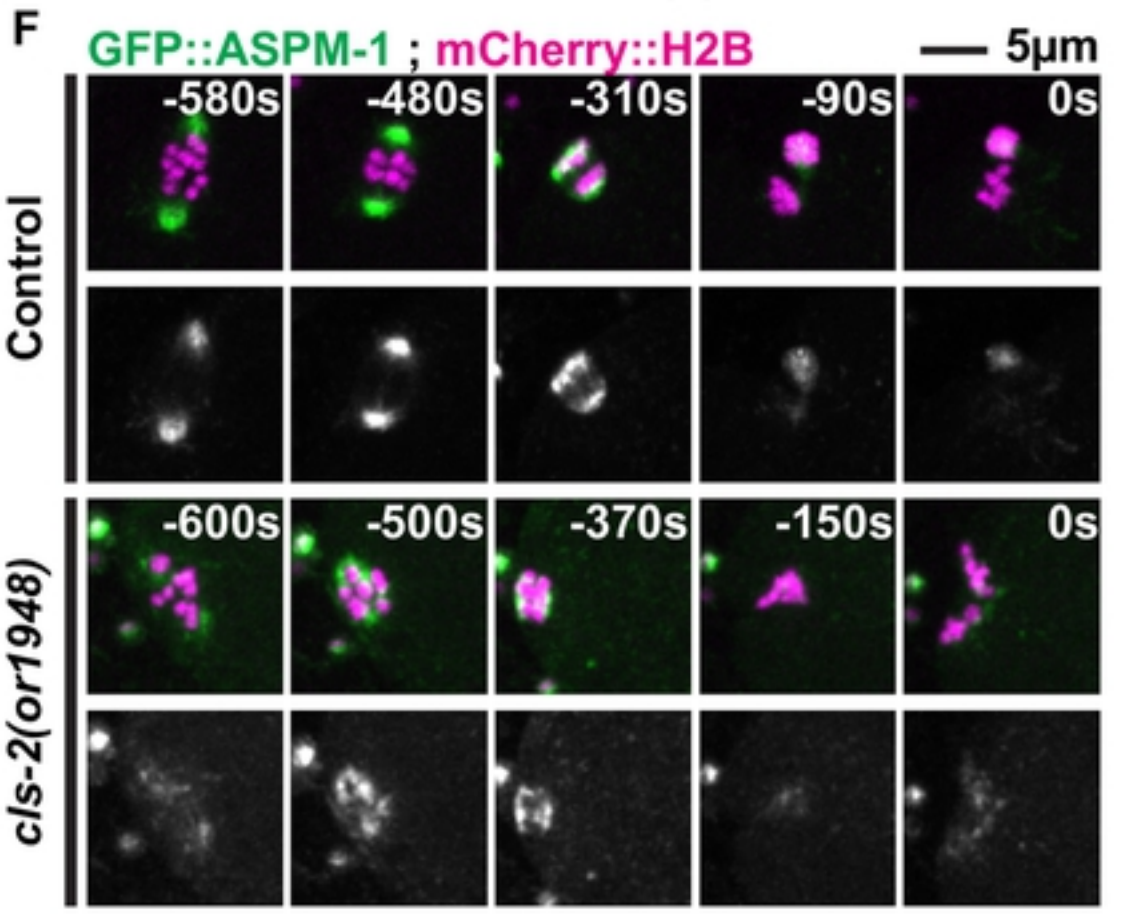

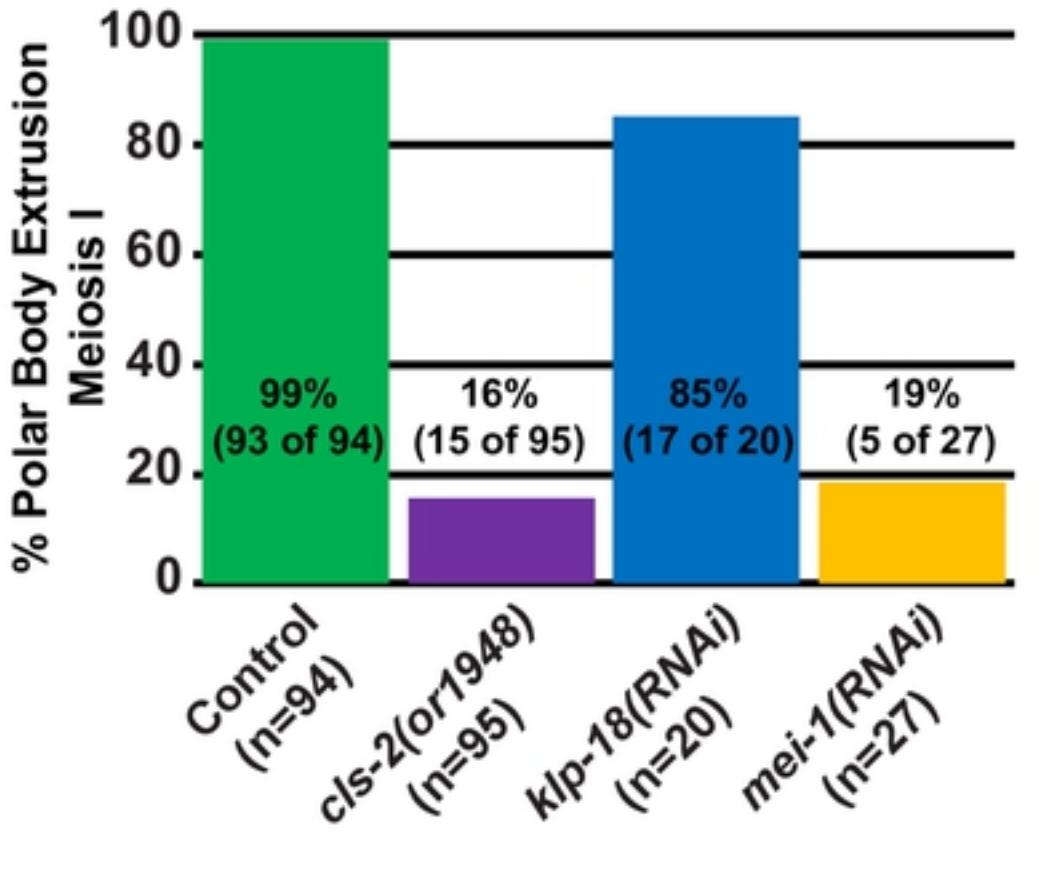

Fig 3

A

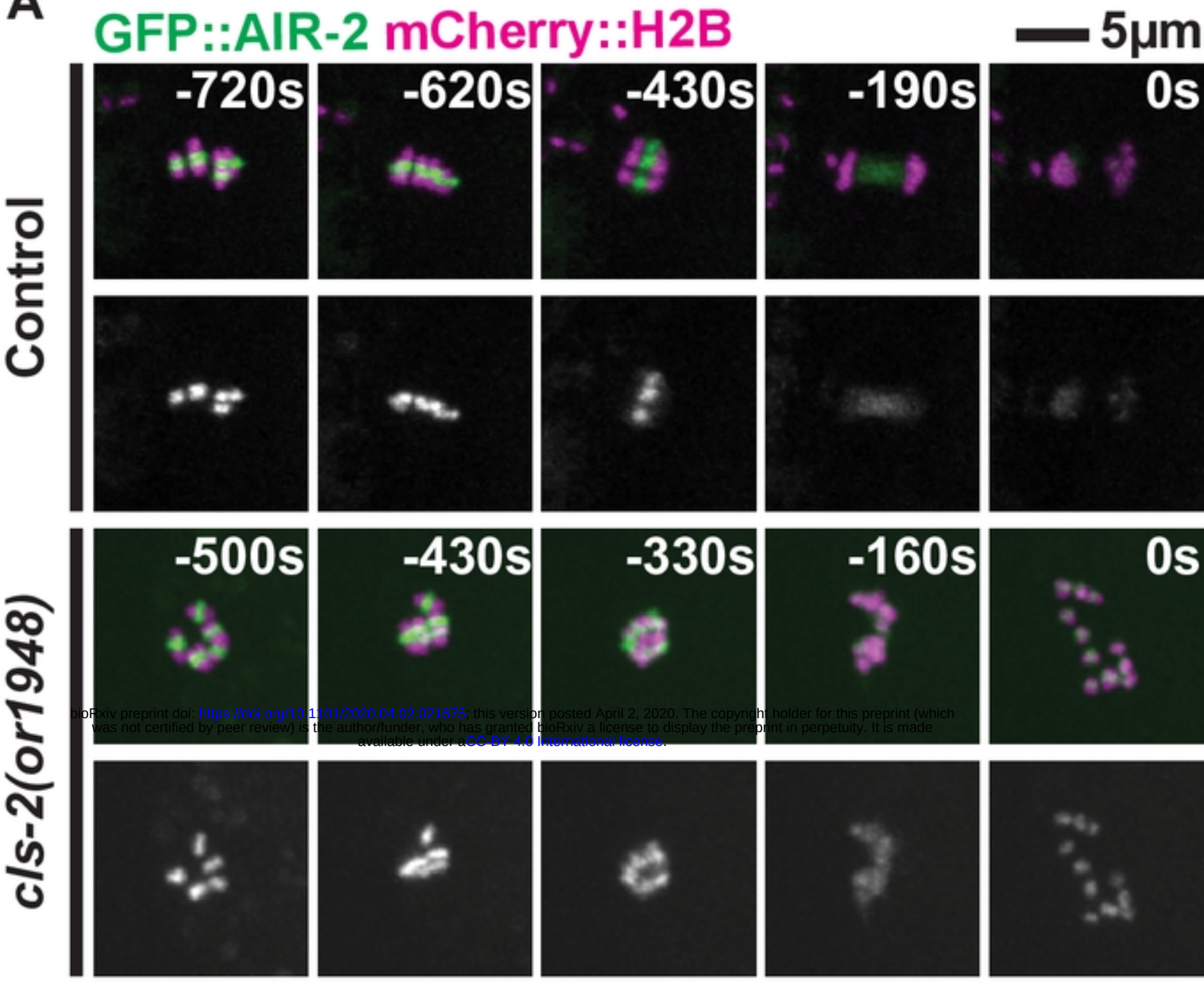

B

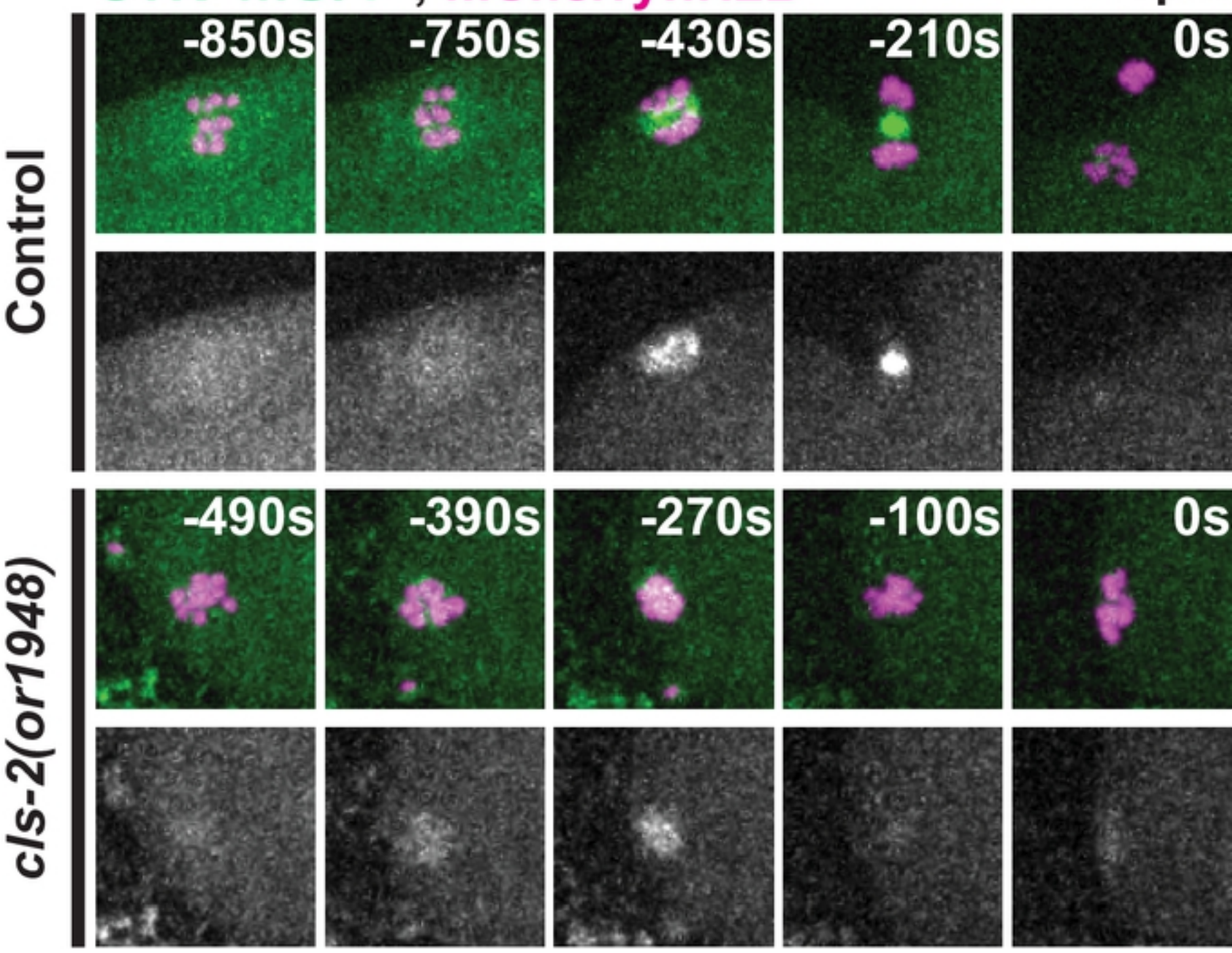

Fig 3

Fig 4

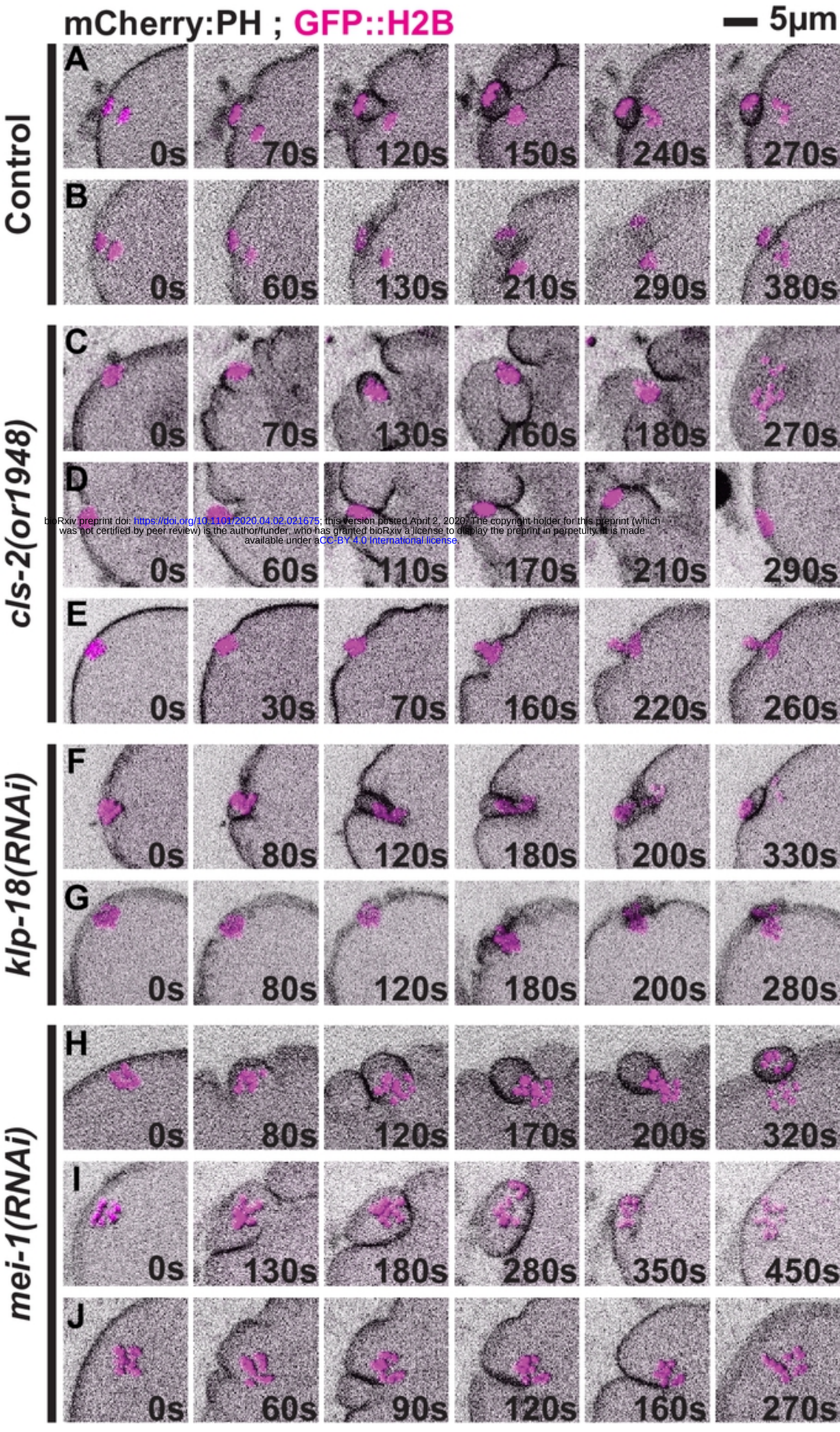

Fig 4

Fig 5

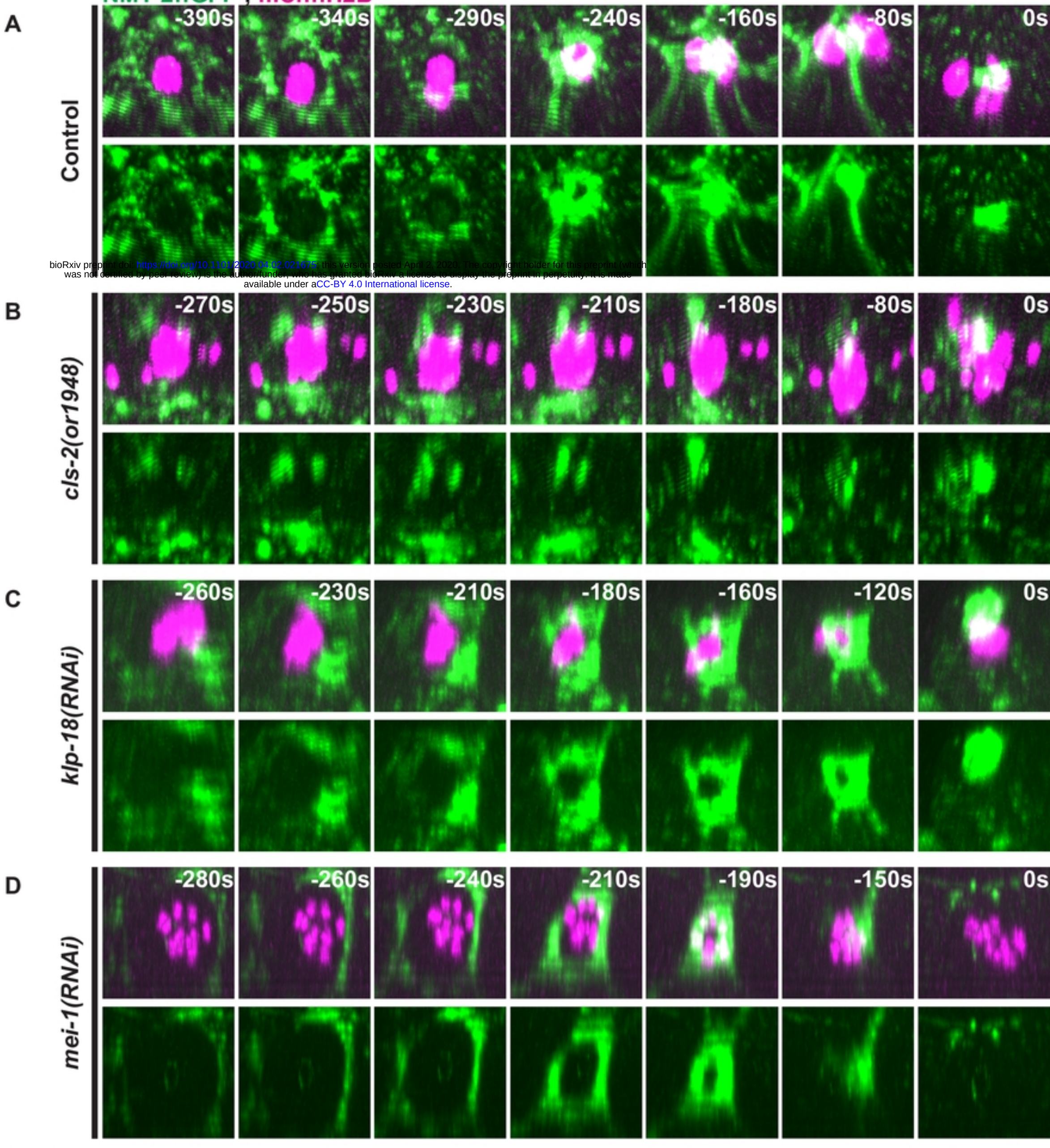

Fig 5

Fig 6

A

mNeonGreen::ANI-1 ; mCh::H2B

Control

-320s -270s -230s -200s -160s -70s 0s

cls-2(or1948)

-270s -240s -220s -190s -170s -120s 0s

B

NMY-2::mKate2 ; mNeonGreen::ANI-1 ; mCh::H2B

Control

-250s -220s -200s -180s -160s -100s 0s

cls-2(or1948)

-270s -240s -210s -170s -140s -80s 0s

Fig 6

Fig 7

A

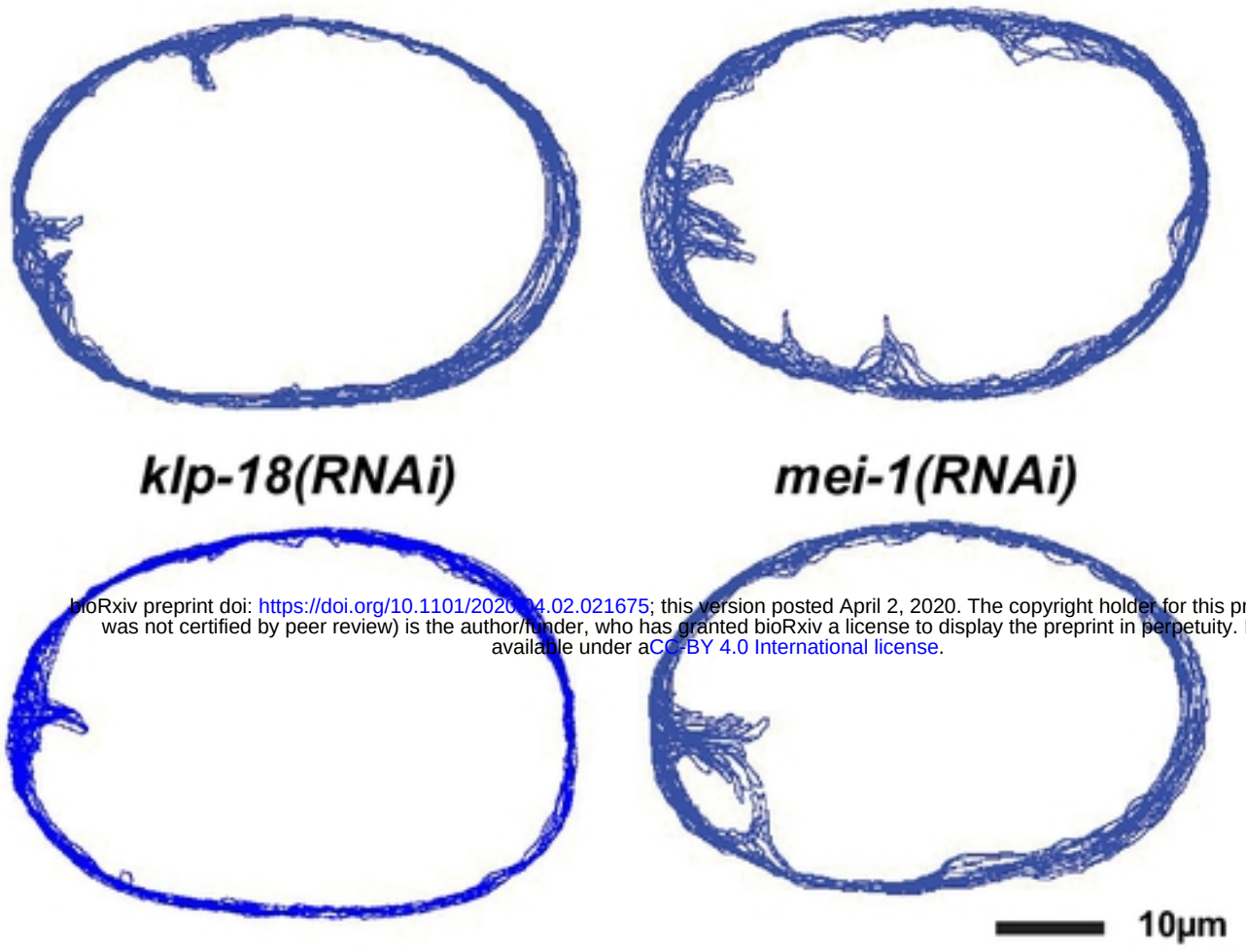

B

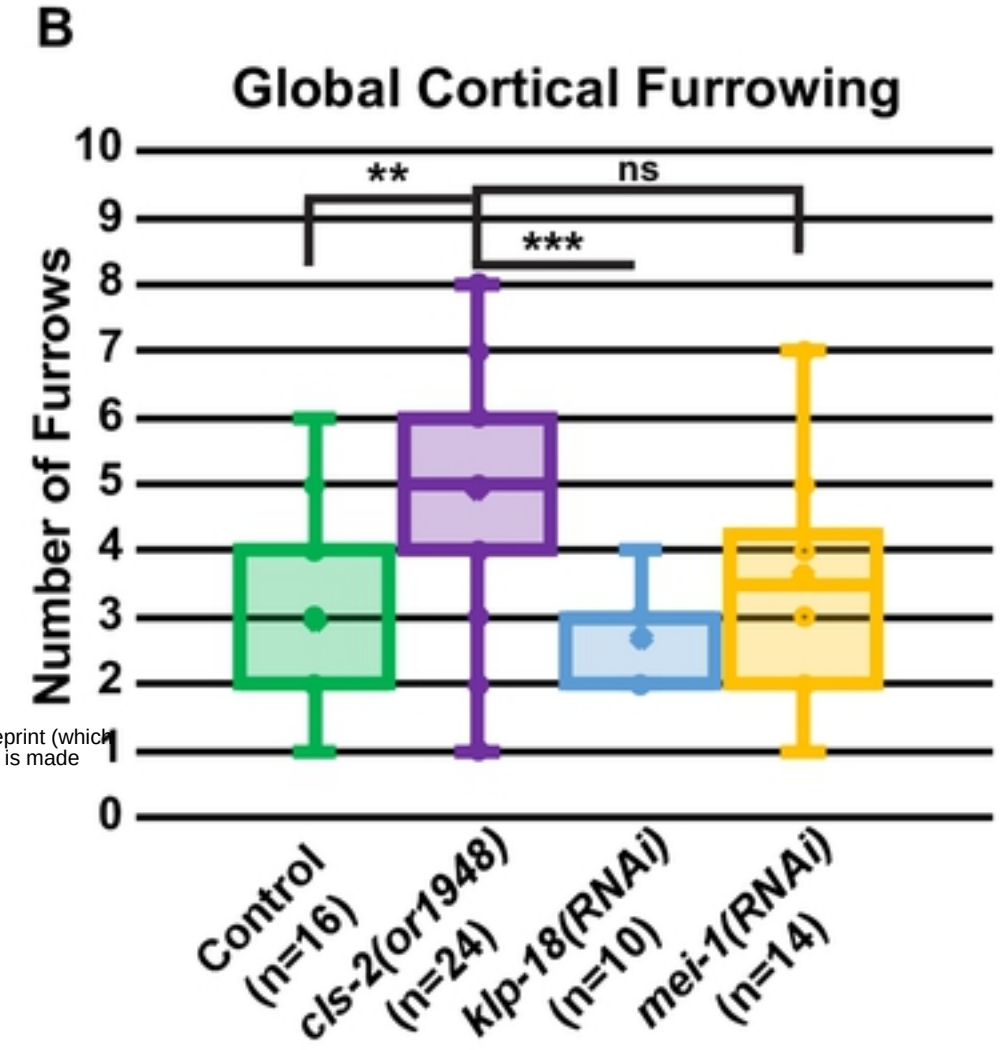

C

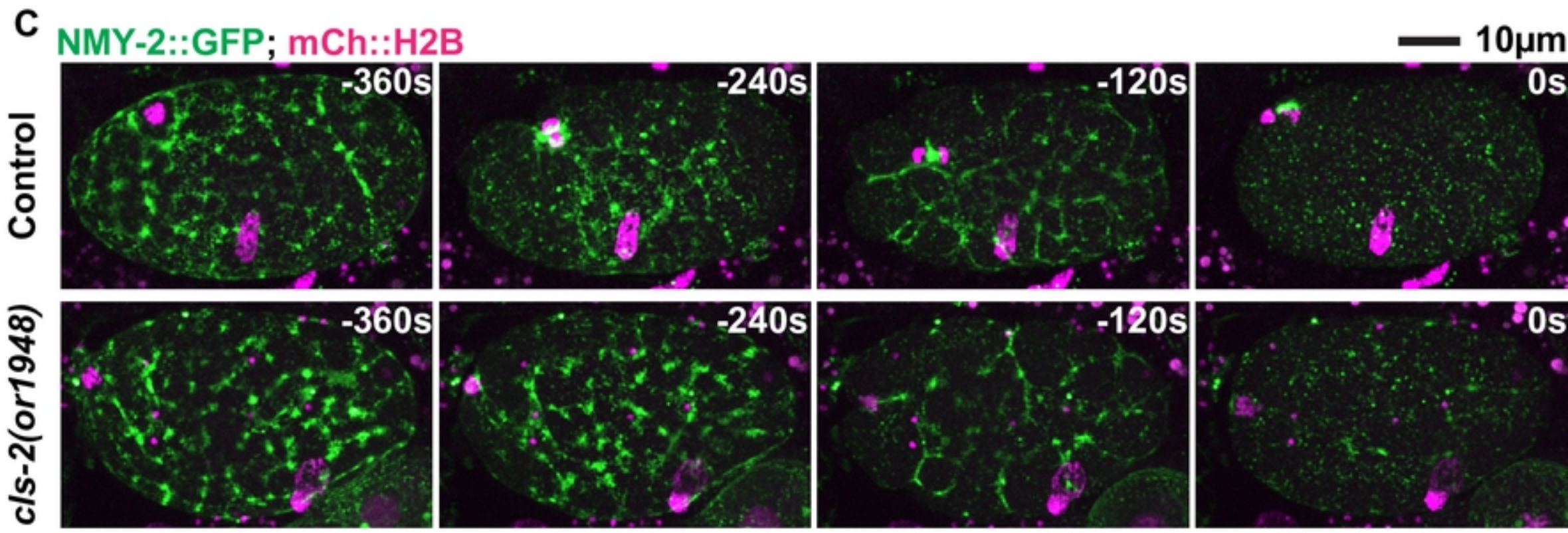

D

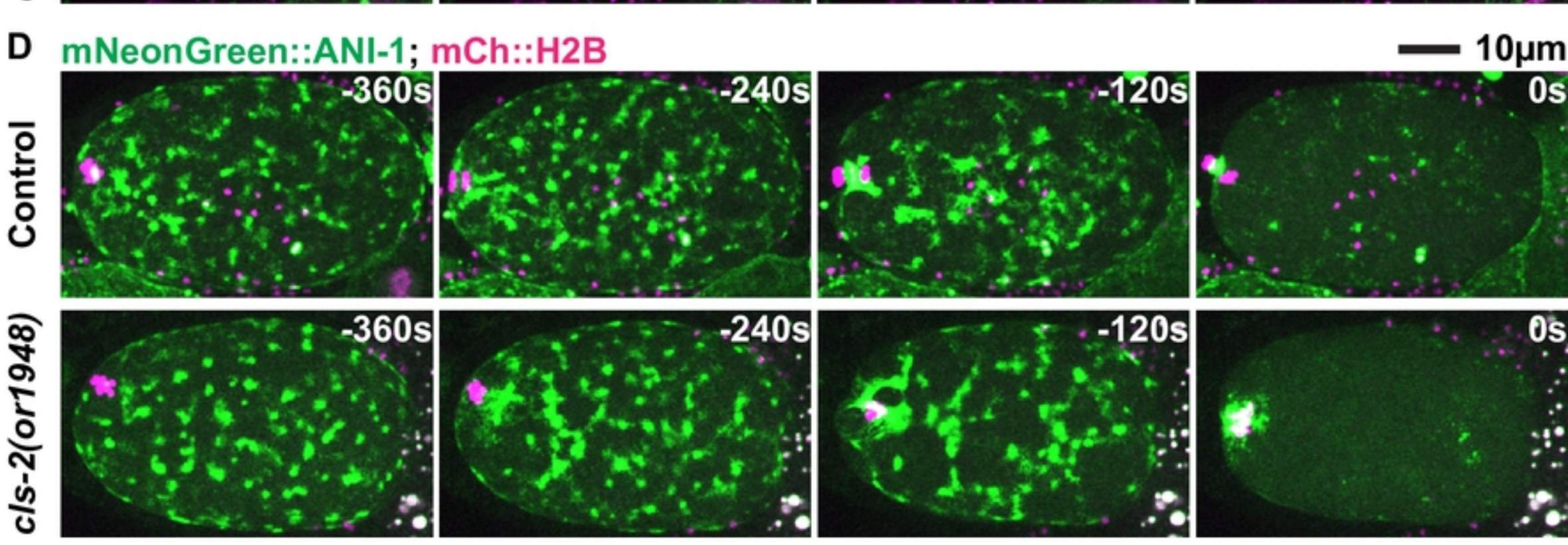

Fig 7